

1 2020 - 07- 16

2 To the Editor of "CLIMATE OF THE PAST"

3
4 Dear Dr. Paul / Dear André,

5
6 Thank you for the fast editor's decision of June 24 (copy attached) and his helpful
7 detailed comments. In response, we now like to comment on the editor's
8 three remaining major points, the first one is actually critical for finally accepting your manuscript for publication:
9 (1) Unpublished data and manuscripts "in prep."

10 There are two unpublished data sets related to two manuscripts by Ausin et al. and Küssner et al. that are
11 both still "in prep." (by the way, the manuscript by Ausin et al. is not even cited). The data sets are stored at
12 PANGAEA, but "under embargo as the papers are still in preparation", hence they are not yet available in any
13 way, and therefore it is impossible to evaluate them. Both the referee and myself expressed that we are not
14 satisfied with this situation. We understand that it is highly frustrating for you as authors of this manuscript,
15 too. However, in its current form it cannot be published using those data.

16 With regard to the four options proposed by the editor to cope with the "difficult
17 situation" of our manuscript, we decided to ask for option (a), that is, to put our
18 manuscript "on hold" until the two manuscripts of Küssner et al. and of Ausin et al. will
19 have been submitted to a peer-reviewed journal and the embargo on the related data
20 sets on PANGAEA will be lifted. In both cases the authors are working hard to
21 finalize their manuscripts soon over the upcoming weeks.

22 (2) Personal communication ("pers. com")

23 On several occasions, you refer to unpublished, personal communications. As there is no way to check those
24 for correctness, I ask you to remove all personal communications from the text and rephrase the text accordingly. If you
25 want, you can still mention the persons you talked to in the Acknowledgment section.

26 To cope with this problem of three unpublished personal communications we are happy
27 to follow the editor's suggestion to replace that of Bronk Ramsey (former line 249) by a
28 reference to his paper now published under 2020, that of Butzin (former line 574) by a
29 wording proposed by the editor himself to replace our own wording of former lines 572–
30 577, and that of Abé-Ouchi by a reference to her abstract for the OC3/IPODS Meeting
31 held in Cambridge in September 2018.

32 (3) Length of manuscript

33 Another issue is the sheer length of the manuscript, which is 850 lines plus 100 lines and a couple of figures
34 in the supplement. Attempts to shorten the manuscripts as recommended by the referees and myself have
35 only been partly successful. Therefore, I would welcome further attempts to shorten, for example, the
36 abstract and the introduction.

37 We now shortened the abstract by 10% (by 2 lines) and the introduction by 14% (by 36
38 lines). A one-page abstract (now 343 w.) may be appropriate for a major synthesis
39 paper. Pertinent text sections are marked-up RED in the revised manuscript. With
40 regard to the overall file size, we'd like to mention that we transferred several figs. from
41 the Suppl. Materials to the main manuscript following the advice of a reviewer.

42
43 With sincere thanks for your care in editing and helpful suggestions, and kind regards,

44
45 Michael Sarnthein and coauthors

46
47

48 Plateaus and jumps in the atmospheric radiocarbon record – Potential origin and value
49 as global age markers for glacial-to-deglacial paleoceanography, a synthesis

50

51

52 Michael Sarnthein¹⁾, Kevin Küssner²⁾, Pieter M. Grootes³⁾, Blanca Ausin⁴⁾⁸⁾, Timothy
53 Eglinton⁸⁾, Juan Muglia⁵⁾, Raimund Muscheler⁶⁾, Gordon Scholout⁷⁾

54

55

56 1) Institute of Geosciences, University of Kiel, Olshausenstr. 40, 24098 Kiel, Germany,
57 michael.sarnthein@ifg.uni-kiel.de, (corresponding author)

58 2) Alfred-Wegener-Institut Helmholtz-Zentrum für Polar- und Meeresforschung,
59 Department for Marine Geology, 27570 Bremerhaven, Germany, kevin.kuessner@awi.de

60 3) Institute of Ecosystem Research, University of Kiel, Olshausenstr. 40, 24098 Kiel,
61 Germany, pgrootes@ecology.uni-kiel.de

62 4) Geology Department, University of Salamanca, Plaza de los Caldos, 37008
63 Salamanca, Spain, <ausin@usal.es>

64 5) Centro para el Estudio de los Sistemas Marinos, CONICET, 2915 Boulevard Brown,
65 U9120ACD, Puerto Madryn, Argentina, jmuglia@cenpat-conicet.gob.ar

66 6) Quaternary Sciences, Department of Geology Lund University, Sölvegatan 12, 22362
67 Lund, Sweden, raimund.muscheler@geol.lu.se

68 7) Climate Dynamics and Landscape Evolution, GFZ German Centre for Geosciences,
69 Telegrafenberg, 14473 Potsdam, Germany, ScholoutG@gmail.com

70 8) Geological Institute, ETH Zürich, Sonneggstr. 5, 8092 Zuerich, Switzerland,

71

72

73

74

75 ABSTRACT

76 Changes in the geometry of ocean Meridional Overturning Circulation (MOC) are crucial in
77 controlling past changes of climate and the carbon inventory of the atmosphere. However, the
78 accurate timing and global correlation of short-term glacial-to-deglacial changes of MOC in
79 different ocean basins still present a major challenge. The fine structure of jumps and plateaus
80 in atmospheric and planktic radiocarbon (^{14}C) concentration reflects changes in atmospheric ^{14}C
81 production, ocean-atmosphere ^{14}C exchange, and ocean mixing. Plateau boundaries in the
82 atmospheric ^{14}C record of Lake Suigetsu, now tied to Hulu U/Th model-ages instead of optical
83 varve counts, provide a stratigraphic 'rung ladder' of up to 30 age tie points 29 to 10 cal. ka for
84 accurate dating of planktic oceanic ^{14}C records. The age differences between contemporary
85 planktic and atmospheric ^{14}C plateaus record the global distribution of ^{14}C reservoir ages for
86 surface waters of the Last Glacial Maximum (LGM) / deglacial Heinrich Stadial 1 (HS-1), as
87 documented in 19/20 planktic ^{14}C records. Elevated and variable reservoir ages mark both
88 upwelling regions and high-latitude sites covered by sea ice and/or meltwater. ^{14}C ventilation
89 ages of LGM deep waters reveal opposed geometries of Atlantic and Pacific MOC. Like today,
90 Atlantic deep-water formation went along with an estuarine inflow of old abyssal waters from the
91 Southern Ocean up to the northern North Pacific and an outflow of upper deep waters. During
92 early HS-1, ^{14}C ventilation ages suggest a reversed MOC and ~1500 year-long flushing of the
93 deep North Pacific up to the South China Sea, when estuarine circulation geometry marked the
94 North Atlantic, gradually starting near 19 ka. High ^{14}C ventilation ages of LGM deep waters
95 reflect a major drawdown of carbon from the atmosphere. The subsequent major deglacial age
96 drop reflects changes in MOC accompanied by massive carbon releases to the atmosphere as
97 recorded in Antarctic ice cores. These new features of MOC and the carbon cycle provide
98 detailed evidence in space and time to test and refine ocean models that, in part because of
99 insufficient spatial model resolution and reference data, still poorly reproduce our data sets.

100

101

102 1. INTRODUCTION

103 1.1 A variety of terms linked to the notion '14C age'

104 The ¹⁴C concentration in the troposphere is mainly determined by ¹⁴C production,
105 atmospheric mixing, moreover, air-sea gas exchange and ocean circulation that vary
106 over time (e.g., Alves et al., 2018; Alveson et al., 2018). The ¹⁴C content of living
107 terrestrial plants is in equilibrium with the atmosphere via processes of photosynthesis
108 and respiration. Accordingly, the ¹⁴C of terrestrial plant remains in a sediment section
109 directly reflects the amount of radioactive decay, thus the time passed since the plant's
110 death, and the ¹⁴C composition of the atmosphere during the time of plant growth.

111

112 Contrariwise, ¹⁴C values of marine and inland waters are cut off from cosmogenic ¹⁴C
113 production in the atmosphere, hence depend on the carbon transfer at the air-water
114 interface and the result of local transport and mixing of carbon in the water. For surface
115 waters, the air-sea transfer involves a time span of ten years and less (e.g., Nydal et al.,
116 1998). Yet, vertical and horizontal water mixing results in surface ocean ¹⁴C
117 concentrations on average 5 % lower than those in the contemporaneous atmosphere,
118 a difference expressed as 'Marine Reservoir Age' (or 'reservoir effect' *sensu* Alves et
119 al., 2018). These 'ages' reflect the local oceanography and are highly variable through
120 time (~200–2500 yr; e.g., Stuiver and Braziunas, 1993; Grootes and Sarnthein, 2006;
121 Sarnthein et al., 2015). Apart from U/Th dated corals (many papers on their reservoir
122 age since Adkins and Boyle, 1997), the ¹⁴C age of planktic foraminifers is the most
123 common tracer in marine sediments providing a rough estimate of the time passed
124 since sediment deposition. Soon, however, marine geologists were confronted with age
125 inconsistencies that implied a series of unknowns, in particular the surface ocean ¹⁴C
126 'reservoir age' that finally became a most valuable tracer for oceanography.

127

128 The ^{14}C records of benthic foraminifers in deep-sea sediments reflect the time of
129 radioactive decay since their deposition with the apparent 'ventilation age' of the deep
130 waters in which they lived. Ventilation age is primarily the time span from the moment
131 when carbon dissolved in the local surface waters with somewhat reduced ^{14}C level lost
132 contact with the atmosphere until the precipitation of benthic carbonate from the down-
133 welled deep waters. Details on the derivation of ventilation ages are provided in Cook
134 and Keigwin (2015) and Balmer and Sarnthein (2018). In addition, however, ventilation
135 ages include hardly quantifiable lateral admixtures of older and/or younger water
136 masses, moreover, ^{14}C -enriched organic carbon supplied by the biological pump, thus
137 are called 'apparent'. Today, the apparent transit times of carbon dissolved in the deep
138 ocean range from a few hundred up to ~ 1800 ^{14}C yr found in upper deep waters of the
139 northeastern North Pacific (Matsumoto, 2007).

140

141 The reservoir ages of surface waters and the ventilation ages of deep waters present
142 robust and high-resolution tracers essential for drawing quantitative conclusions on past
143 ocean circulation geometries, marine climate change, and the processes that drive both
144 past ocean dynamics and carbon budgets, given the ages rely on a number of robust
145 age tie points. Obtaining such tie points presents a problem, since any attempt to date a
146 deep-sea sediment record by means of ^{14}C encounters a number of intricacies of how to
147 disentangle the effects of global atmospheric ^{14}C variations due to past changes in
148 cosmogenic ^{14}C production and carbon cycle from (i) local depositional effects such as
149 sediment hiatuses and winnowing, differential bioturbational mixing depth, and sediment
150 transport by deep burrows, (ii) the effects of local atmosphere-ocean exchange and
151 ocean mixing resulting in reservoir and ventilation ages that change through time and

152 space (e.g., Alves et al. 2018; Grootes and Sarnthein, 2006), and (iii) from the final
153 target, quantitatively 'pure' ^{14}C ages due to radioactive decay. These problems are
154 exacerbated by the need for a generally accepted high-precision atmospheric reference
155 record for the period 14–50 cal. ka, beyond tree ring calibration,
156
157 Current ^{14}C -based chronologies of deep-sea sediment records, used to constrain and
158 correlate the age of glacial-to-deglacial changes in ocean dynamics and climate on a
159 global scale, are often of insufficient quality when they are based on (i) age tie points
160 spaced far too wide (e.g., using DO-events 1, 2, and 3 only and/or sporadic tephra
161 layers for the time span 30–14 cal ka), (ii) disregarding atmospheric ^{14}C plateaus, (iii)
162 the risky assumption of \pm constant planktic ^{14}C reservoir ages and other speculative
163 stratigraphic correlations/compilations, and (iv) ignoring small-scale major differences in
164 low-latitude reservoir age. Likewise, clear conclusions are precluded by an uncertainty
165 range of 3-4 kyr sometimes accepted for tie points during the glacial-to-deglacial period
166 (Stern and Lisiecki, 2013; Lisiecki and Stern, 2016), where significant global climate
167 oscillations occurred on decadal-to-centennial time scales as widely shown on the basis
168 of speleothem and ice core-based records (Steffensen et al., 2008; Svensson et al.,
169 2008; Wang et al., 2001). Thus marine paleoclimate and paleoceanographic studies
170 today focus on the continuing quest for a high-resolution and global, hence necessarily
171 atmospheric ^{14}C reference record.

172

173 *1.2 Review of tie points used to fix calibrated and reservoir ages in marine ^{14}C records*

174 The tree ring-based calibration of ^{14}C ages provides a master record of decadal
175 changes in atmospheric ^{14}C concentrations back to ~14 cal. ka (Reimer et al., 2013 and
176 2020) with floating sections beyond (from ~12.5–14.5 cal. ka, around 29–31.5 and 43

177 cal. ka; Turney et al., 2010, 2017, Reimer et al., 2020). The evolution of Holocene and
178 late deglacial ^{14}C ages with time is not linear but reveals variations with numerous
179 distinct jumps (= rapid change) and (short) plateau-shaped (slow or no change or even
180 inversion) structures indicative of fluctuations in atmospheric ^{14}C concentration. Prior to
181 8500 cal. yr BP, various plateaus extend over 400–600 cal. yr and beyond (Fig. 2).
182 Given the quality of the tree ring calibration data, these fluctuations can be considered
183 real, suitable for global correlation (Sarnthein et al., 2007, 2015; Umling and Thunnell,
184 2017; Sarnthein and Werner, 2018). Air-sea gas exchange transfers the atmospheric
185 ^{14}C fluctuations into the surface ocean where they can provide high-resolution tie points
186 to calibrate the marine ^{14}C record and marine reservoir ages back to ~14 ka (via " ^{14}C
187 wiggle matching"). In the near future, however, it is unlikely that a continuous tree ring-
188 based record will become available to trace such atmospheric ^{14}C variations further
189 back, over the period 14–29 cal. ka crucial for the understanding of last-glacial-to-
190 interglacial changes in climate. Hence various other, carbonate-based ^{14}C archives
191 have been employed for this period to reconstruct past changes in atmospheric ^{14}C
192 concentration/age and tie them to an 'absolute' or 'calibrated' (e.g., incremental and/or
193 based on speleothem carbonate) age scale.

194

195 Suites of ^{14}C ages of paired marine and terrestrial plant-borne samples, e.g. paired
196 planktic foraminifers and wood chunks, provide most effective but rarely realizable
197 absolute-age markers and reservoir ages of local ocean surface waters (Zhao and
198 Keigwin, 2018; Rafter et al., 2018; Schroeder et al., 2016; Broecker et al., 2004).
199 Likewise successful appears the alignment of ^{14}C -dated variations in downcore sea-
200 surface temperatures (SST) with changes in hydroclimate as recorded in age-calibrated
201 sedimentary leaf-wax hydrogen isotope (δD) records from ancient lakes (Muschitiello et

202 al., 2019), assumed to be coeval. Further tie points are derived from volcanic ash layers
203 (Waelbroeck et al., 2001; Siani et al., 2013; Davies et al., 2014; Sikes and Guilderson,
204 2016), paired U/Th- and ^{14}C -based coral ages (Adkins and Boyle, 1997; Robinson et al.,
205 2005; Burke and Robinson, 2012; Chen et al., 2015), and the (fairly fragmentary)
206 alignment of major tipping points in ^{14}C dated records of marine SST and planktic $\delta^{18}\text{O}$
207 to the incremental age scale of climate events dated in polar ice core records
208 (Waelbroeck et al., 2011). Such well-defined tie points, however, are wide-spaced in
209 peak glacial-to-early deglacial ice core records, too wide for properly resolving a clear
210 picture of the spatiotemporal pattern of marine paleoclimate events. Finally, various
211 data compilations tentatively rely on the use of multiple age correlations amongst
212 likewise poorly dated marine sediment records, an effort necessarily problematic.
213 Skinner et al. (2019) recently combined new and existing reservoir age estimates from
214 North Atlantic and Southern Ocean to show coherent but distinct regional reservoir age
215 trends in subpolar ocean regions, trends that indeed envelop the range of actual major
216 small-scale and short-term oscillations in reservoir age revealed by our technique of ^{14}C
217 plateau tuning for the subpolar South Pacific (Küssner et al., 2020 subm.).
218
219 Lacking robust age tie points several authors resort to ^{14}C reservoir age simulations for
220 various sea regions by ocean General Circulation Models (GCM) (e.g. Butzin et al.,
221 2017; Muglia et al., 2018) to quantify the potential difference between marine and
222 atmospheric ^{14}C dates for glacial-to-interglacial times. In view of the complexity of ocean
223 MOC and the global carbon cycle it is not surprising that the results of a comparison of
224 a selection of robust empiric vs. simulated ^{14}C reservoir ages are not that encouraging
225 yet (as discussed further below).

226

227 Beyond accepting a generally close link between ^{14}C concentrations in the troposphere
228 and in the surface ocean, the fine structure of planktic ^{14}C records with centennial-scale-
229 resolution can provide a far superior (though costly) link of the marine sediment records
230 to the reference suite of narrow-standing jumps and boundaries of the plateaus robustly
231 identified in the atmospheric ^{14}C record of Lake Suigetsu, the only long, continuous
232 record based on terrestrial plant remains (Bronk Ramsey et al., 2012, 2019). Beyond
233 the reach of the tree ring-based age scale ~ 14 cal. ka, the absolute age of the Suigetsu
234 atmospheric ^{14}C structures can be either calibrated by incremental (microscopy- or
235 XRF-based) varve counts (Scholaut et al., 2018; Marshall et al., 2012) or by a series of
236 paired U/Th- and ^{14}C -based model ages correlated from the Hulu Cave speleothem
237 record (Bronk Ramsey, 2012 and 2019; Southon et al., 2012; Cheng et al., 2018). The
238 difference in absolute age between these calibrations (Fig. 3) is of little importance for
239 the tuning of planktic to corresponding atmospheric ^{14}C plateaus and the derivation of
240 planktic reservoir ages that present the highly variable offset of the ^{14}C age of a planktic
241 plateau from that of the correlated atmospheric plateau. The offset is deduced by
242 subtracting the average ^{14}C age of an atmospheric ^{14}C plateau from that of the
243 correlated planktic ^{14}C plateau, independent of any absolute age value assigned.

244

245 The uncertainty of the Suigetsu atmospheric ^{14}C record is significantly larger than that
246 of the tree ring-based calibration record because of lower ^{14}C concentrations, limited
247 sampling density, and uncertainties in the independent age determination. Thus the ^{14}C
248 fluctuations could be real or represent mere statistical scatter (null hypothesis) in which
249 case the record of atmospheric ^{14}C ages against time would show a simple continuous
250 rise resulting from radioactive decay and the advance of time, such as suggested by a

251 fairly straight progression of the highly resolved deglacial Hulu Cave ^{14}C record plotted
252 vs. U/Th ages (Southon et al., 2012; Cheng et al., 2018).

253

254 The unequivocal fluctuations in the tree ring-based master record of atmospheric ^{14}C
255 concentration (Fig. 2; Reimer et al., 2013, 2020) are on the order of 2–3 % over the last
256 10 kyr (Stuiver and Braziunas, 1993) and even larger back to ~14 ka. Under glacial and
257 deglacial low- CO_2 conditions beyond 14 ka, when climate and ocean dynamics were
258 less constant than during the Holocene, real atmospheric ^{14}C fluctuations were, most
259 likely, even stronger and ^{14}C plateaus and jumps accordingly larger. Plateau-jump
260 structures are also becoming increasingly evident in the evolving atmospheric
261 calibration record (Reimer et al., 2020). The age-defined plateaus and jumps in the
262 Suigetsu atmospheric ^{14}C calibration curve may thus be regarded as a suite of ‘real’
263 structures, extending the calibration provided by the tree ring record for Holocene and
264 B/A-to-Early Holocene times (Fig. 2) into early deglacial and LGM times.

265

266 The plateau/jump structures may partly be linked to changes in cosmogenic ^{14}C
267 production, as possibly shown in the ^{10}Be record (Fig. 4; based on data of Adolphi et al.,
268 2018), and – presumably more dominant – to short-term changes in ocean mixing and
269 the carbon exchange between ocean and atmosphere. The exchange is crucial, since
270 the carbon reservoir of the ocean contains up to 60 (preindustrial) atmospheric carbon
271 units (Berger and Keir, 1984). The apparent contradiction with the smooth Hulu Cave
272 ^{14}C record (Southon et al., 2012; Cheng et al., 2018) may possibly be explained by the
273 Hulu Cave speleothem precipitation system acting as a low-pass filter for fluctuating
274 atmospheric ^{14}C concentrations (statistical tests of Bronk Ramsey et al., pers. comm.
275 2018) and, to a very limited degree, by the obvious scatter in the Suigetsu data. The

276 filter for Hulu data possibly led to a loss especially of short-lived structures in the
277 preserved atmospheric ^{14}C record, though some remainders were preserved in the ^{14}C
278 records of Hulu Cave (Fig. 1). So we rather trust the amplitude of Suigetsu ^{14}C
279 structures than the timing of Hulu Cave data.

280

281 Like a 'rung ladder' the age-calibrated suite of ^{14}C plateau boundaries and jumps is
282 suited for tracing the calibrated age of numerous plateau boundaries in glacial-to-
283 deglacial marine ^{14}C records likewise densely sampled, even when some rungs have
284 been destroyed by local influences on gas exchange or ocean mixing. Also, one may
285 record the average offset of planktic ^{14}C ages from paired atmospheric ^{14}C ages, i.e. the
286 planktic reservoir age, for each single ^{14}C plateau (Sarnthein et al., 2007, 2015). We
287 prefer the Suigetsu record to IntCal, since it is based on original primary atmospheric
288 data and results in small-scale spatio-temporal changes of reservoir age, whereas
289 IntCal is mixing and smoothing a broad array of different data sources with comparativ-
290 ely coarse age resolution, including carbonate-based speleothem and marine records.
291 For the first time, this suite of tie points may facilitate a precise temporal correlation of
292 all sorts of changes in surface and deep-water composition on a global scale, crucial for
293 a better understanding of past changes in ocean and climate dynamics.

294

295 *1.3 Items discussed in this synthesis*

296 The Results Section is summarizing (1) Means to separate noise, global atmospheric
297 and local oceanic forcings that together control the structure of a planktic ^{14}C plateaus,
298 (2) The choice of a U/Th-based reference time scale (Bronk Ramsey et al. 2012; Cheng
299 et al., 2018) instead of the earlier varve-counted version (Schlolut et al., 2018) to date
300 the structures in the global atmospheric ^{14}C record of Lake Suigetsu (Sarnthein et al.,

301 2015), (3) The extension of the suite of age tie points from 23 back to 29 cal. ka, values
302 crucial for an accurate global correlation of ocean events over the Last Glacial
303 Maximum, and (4) Potential linkages of atmospheric ^{14}C plateaus and jumps to
304 cosmogenic ^{14}C production and/or ocean dynamics.

305

306 The Discussion and Implications section includes:

307 (1) A global summary of published marine ^{14}C reservoir age records (Sarnthein et al.
308 2015) now enlarged by nine plateau-tuned records from the Southern Hemisphere
309 (Balmer et al., 2016 and 2018; Küssner et al., 2018 and 2020 subm.) and the northeast
310 Atlantic (Ausin et al., 2020 subm.). In total, 18 (LGM) / 19 (HS-1) plus three wood
311 chunk-based records (Broecker et al., 2004; Zhao et al., 2018) now depict the spatio-
312 temporal variability of past reservoir ages of surface waters in different ocean regions.
313 (2) A comparison of our plateau-based reservoir ages with LGM estimates of surface
314 water ^{14}C reservoir ages simulated by the GCM of Muglia et al. (2018).
315 (3) More detailed insights into the origin of past changes in the global carbon cycle from
316 glacial to interglacial times are provided by the enlarged set of ^{14}C reservoir and venti-
317 lation ages that form a robust tracer of global circulation geometries and the inorganic
318 carbon (DIC) dissolved in different basins of the ocean (Sarnthein et al., 2013).

319

320 The discussion highlights ^{14}C plateau tuning and its revised cal. time scale for global
321 data-model intercomparison and a new understanding of Ocean MOC during the LGM
322 and its reversal during HS-1.

323

324 **2. RESULTS – AGE TIE POINTS BASED ON ^{14}C PLATEAU BOUNDARIES**

325

326 2.1 *Suite of planktic ¹⁴C plateaus: Means to separate global atmospheric from local*
327 *oceanographic forcings*

328 The basic assumption of the ¹⁴C plateau tuning technique is that the fine structure of
329 fluctuations of the global atmospheric ¹⁴C concentration record can also be found in the
330 surface ocean. In a plot of ¹⁴C age versus calendar age such fluctuations lead to a pattern
331 of plateaus/jumps that correspond to decreases/increases in ¹⁴C concentration. Here we
332 refer to the derivation and interpretation of planktic ¹⁴C plateaus, assuming a predom-
333 inantly global atmospheric origin with occasional local oceanographic forcings. The series
334 of planktic ¹⁴C plateaus and jumps are derived in cores with average hemipelagic
335 sedimentation rates of >10 cm/ky and dating resolution of <100-150 yr. The plateau-
336 specific structures in a sediment age-depth record form a well-defined suite for which
337 absolute age and reservoir age are derived by means of a strict alignment to the reference
338 suite of global atmospheric ¹⁴C plateaus as a whole. Initially, age tie points of planktic
339 foraminiferal $\delta^{18}\text{O}$ records showing (orbital) isotope stages #1-3 serve as stratigraphic
340 guideline for the alignment under the simplifying assumption that stratigraphic gaps are
341 absent, not always true (Suppl. Fig. 2). Planktic reservoir ages and their short-term
342 changes are derived from the difference in average ¹⁴C age between atmosphere and
343 surface waters in subsequent plateaus. To stick as close as possible to the modern range
344 of reservoir ages (Stuiver and Braziunas, 1993), tuned reservoir ages are kept at a
345 minimum unless stringent evidence requires otherwise.

346

347 A close correspondence between ¹⁴C concentrations in atmosphere and surface ocean
348 is expected based on rapid gas exchange. In several cases, however, the specific
349 structure and relative length of a planktic ¹⁴C plateau may deviate from those of the
350 pertinent plateau observed within the suite of atmospheric plateaus, thus indicate local

351 intra-plateau changes of reservoir age. Though less frequent, these changes may indeed
352 amputate and/or deform a plateau, then as result of variations in local ocean atmosphere
353 exchange and oceanic mixing. Two aspects help to sort out short-term climate-driven
354 intra- and inter-plateau changes in ^{14}C reservoir age: (i) The evaluation of the structure
355 and reservoir age of an individual plateau is strictly including the age estimates deduced
356 for the complete suite of plateaus. (ii) Our experience shows that deglacial climate
357 regimes in control of changes in surface ocean dynamics generally occurred on (multi-)
358 millennial time scales (e.g., YD, B/A, HS-1), whereas atmospheric ^{14}C plateaus hardly
359 lasted longer than a few hundred up to 1100 yr (Fig. 1 and S1). Abrupt changes in gas
360 exchange or ocean mixing usually affect one or only a few plateaus of the suite. --
361 Absolute age estimates within a plateau are derived by linear interpolation between the
362 age of the base and top of an undisturbed plateau assuming constant sedimentation
363 rates. The potential impact of short-term sedimentation pulses on ^{14}C plateau formation
364 has largely been discarded by Balmer and Sarnthein (2016).

365

366 *2.2 Suigetsu atmospheric ^{14}C record: Shift to a chronology based on U/Th model ages*

367 Originally, we based the chronology of ^{14}C plateau boundaries in the Suigetsu record
368 (Sarnthein et al., 2015) on a scheme of varve counts by means of light microscopy of
369 thin sections (Bronk Ramsey et al., 2012; Schlolaut et al., 2018). Over the crucial
370 sediment sections of the Last Glacial Maximum (LGM) and deglacial Heinrich Stadial 1
371 (HS-1), however, varve quality / perceptibility in the Suigetsu profile is highly variable
372 (Fig. 5). In parallel, varve-based age estimates were derived from counting various
373 elemental peaks in μXRF data and interpreted as seasonal signals (Marshall et al.,
374 2012). The results obtained from the two independent counting methods and their
375 interpolations widely support each other but diverge for older ages. The varve counts

376 ultimately formed the backbone of a high-resolution chronology obtained by tying the
377 Suigetsu ^{14}C record to the U/Th based time scale of the Hulu cave ^{14}C record (Bronk
378 Ramsey et al., 2012). Recently, Schlolaut et al. (2018) amended the scheme of varve
379 counts. Accordingly, Suigetsu varve preservation (i.e., the number of siderite layers per
380 20 cm thick sediment section) is fairly high prior to ~ 32 ky BP and over late glacial
381 Termination I but fairly poor over large parts of the LGM and HS-1, from $\sim 15 - 32$ cal ka
382 (17.3-28.5 m c.d. in Fig. 5). Here only less than 20-40 % of the annual layers expected
383 from interpolation between clearly varved sections are distinguished by microscopy.
384 Varve counts that use μXRF data (Marshall et al., 2012) can distinguish subtle changes
385 in seasonal element variations, that are not distinguishable in thin section microscopy,
386 hence result in higher varve numbers especially during early deglacial-to-peak glacial
387 times. Yet, some subtle variations are difficult to distinguish from noise, which adds
388 uncertainty to the μXRF -based counts. Thus, the results from either counting method
389 are subject to uncertainties that rise with increased varve age (Fig. 5).

390

391 Bronk Ramsey et al. (2012) established a third time scale based on ^{14}C wiggle matching
392 to U/Th dated ^{14}C records of the Hulu Cave and Bahama speleothems. In part, this
393 calibrated (cal.) age scale was based on Suigetsu varve counts, in part on the
394 prerequisite of the best-possible fit of a pattern of low-frequency changes in ^{14}C
395 concentration obtained from Suigetsu and Hulu Cave. The two ^{14}C records were fitted
396 within the uncertainty envelope of the Hulu 'Old / Dead Carbon Fraction' (OCF/DCF) of
397 ^{14}C concentration. The uncertainty of this model is still incompletely understood. The
398 U/Th-based age model of Suigetsu may suffer from the wiggle matching of atmospheric
399 ^{14}C ages of Lake Suigetsu with ^{14}C ages of the Hulu Cave (Southon et al., 2012) in case
400 of major short-term changes in atmospheric ^{14}C concentration due to a memory effect of

401 soil organic carbon in carbonate-free regions of the cave overburden. The speleothem-
402 carbonate-based Hulu ages may have been influenced far more strongly by short-term
403 changes in the local DCF than assumed, as suggested by major variations in a paired
404 $\delta^{13}\text{C}$ record, that reach up to 5 ‰, mostly subsequent to short-term changes in past
405 monsoon climate (Kong et al., 2005). The uncertainty regarding the assumption of a
406 constant OCF/DCF (Southon et al. 2012; Cheng et al., 2018) may hamper the age
407 model correlation between Hulu and Suigetsu records and the Suigetsu chronology.
408

409 We compared the results of the two timescales, independently deduced from varve
410 counts, with those of the U/Th-based model age scale using as test case the base of
411 ^{14}C Plateau 2b, the oldest tie point constrained by μXRF -based counts. In contrast to
412 16.4 cal. ka, supposed by optical varve counts, μXRF -based counts suggest an age of
413 ~ 16.9 cal. ka (Marshall et al., 2012; Schlolaut et al., 2018), which matches closely the
414 U/Th-based estimate of 16.93 ka. This is a robust argument for the use of the U/Th-
415 based Suigetsu time scale as 'best possible' age scale to calibrate the age of thirty ^{14}C
416 plateau boundaries (Fig. 1). In its older part, the U/Th model time scale is further
417 corroborated by a decent match of short-term increases in ^{14}C concentration with the
418 low geomagnetic intensity of the Mono Lake and Laschamp events at ~ 34 and
419 41.1 ± 0.35 ka (Lascu et al., 2016), independently dated by other methods. The new
420 U/Th-based model ages of ^{14}C plateau boundaries are significantly higher than our
421 earlier microscopy-based varve ages over HS-1 and LGM, a difference increasing from
422 ~ 200 yr near 15.3 cal. ka to ~ 530 near 17 ka and 2000 yr near ~ 29 ka (Fig. 3).

423

424 Note, any readjustment of the calendar age of a ^{14}C plateau boundary does not entail
425 any change in ^{14}C reservoir ages afore deduced for surface waters by means of the

426 plateau technique (Sarnthein et al., 2007, 2015), since each reservoir age presents the
427 simple difference in average ^{14}C age for one and the same ^{14}C plateau likewise defined
428 in both the Suigetsu atmospheric and planktic ^{14}C records of marine surface waters,
429 independent of the precise position of this plateau on the calendar age scale.

430

431 In view of the recent revision of time scales (Schloll et al., 2018; Bronk Ramsey et al.,
432 2019) we now extended our plateau tuning and now also defined the boundaries and
433 age ranges of ^{14}C plateaus and jumps for the interval ~23–29 cal. ka, which results in a
434 total of ~30 atmospheric age tie points for the time span 10.5–29 cal. ka (Fig. 1;
435 summary in Table 1; following the rules of Sarnthein et al., 2007 and 2015). Prior to 25
436 cal. ka, the definition of ^{14}C plateaus somewhat suffered from an enhanced scatter of
437 raw ^{14}C values of Suigetsu. -- In addition to visual inspection, the ^{14}C jumps and
438 plateaus were also defined with higher statistical objectivity by means of the first-
439 derivative of all trends in the ^{14}C age-to-calendar age relationship (or –core depth
440 relationship, respectively) by using a running kernel window (Sarnthein et al., 2015).

441

442 *2.3 Linkages of short-term structures in the atmospheric ^{14}C record to changes in*
443 *cosmogenic ^{14}C production versus changes in ocean dynamics*

444

445 Potential sources of variability in the atmospheric ^{14}C record have first been discussed
446 by Stuiver and coworkers in the context of Holocene fluctuations deduced from tree ring
447 data (e.g., Stuiver and Braziunas 1993), more recently simulated (e.g., Hain et al.,
448 2014). -- Similar to changes in ^{14}C , variations in ^{10}Be deposition in ice cores reflect past
449 changes in ^{10}Be production as a result of changes in solar activity and the strength of
450 the Earth's magnetic field (Adolphi et al., 2018). If we accept to omit assumptions on the

451 modulation of past ^{14}C concentrations by changes in the global carbon cycle we can
452 calculate the atmospheric ^{14}C changes over last glacial-to-deglacial times with ^{10}Be and
453 a carbon cycle model and convert them into ^{14}C ages (Fig. 4). Changes in climate and
454 carbon cycle, however, over this period necessarily modified the ^{10}Be -based ^{14}C record
455 if included correctly into the modeling. Between 10 and 13.5 cal. ka, the ^{10}Be -modeled
456 ^{14}C record displays a number of plateau structures that appear to match the Suigetsu-
457 based atmospheric ^{14}C plateaus. Between 15 and 29 cal. ka, however, ^{10}Be -based ^{14}C
458 plateaus are more rare and/or less pronounced than those in the Suigetsu record. Most
459 modelled plateaus are far shorter than those displayed in the suite of atmospheric ^{14}C
460 plateaus of Lake Suigetsu (e.g., plateaus near to the top 2a, 2b, top 5a, and 9), except
461 for a distinct equivalent of plateau no. 6a. On the whole, the modelled and observed
462 structures show little coherence. This may indicate that any direct relationship between
463 variations in cosmogenic ^{14}C production and the Suigetsu plateau record is largely
464 obscured by the carbon cycle, uncorrected climate effects on the ^{10}Be deposition,
465 and/or noise in the ^{14}C data. Also, a relatively high uncertainty of the measured ^{10}Be
466 concentrations in the ice, (in many cases $\sim 7\%$; Raisbeck et al., 2017), and a lower
467 sample resolution in the order of 50 to 200 yr may contribute to the smoothed character
468 of the ^{10}Be record in Fig. 4.

469

470 On the other hand, the 'new' U/Th-based cal. ages of plateau boundaries may suggest
471 some reasonable stratigraphic correlations between peak glacial and deglacial change in
472 atmospheric CO_2 and ^{14}C plateaus with millennial-scale events in paleoceanography (Fig.
473 6, Table 2): The suite of deglacial ^{14}C plateaus no. 2a, 1, and Top YD indeed displays a
474 temporal match with three brief but major deglacial jumps in ocean degassing of CO_2
475 documented in the WDC ice core (Marcott et al., 2014). The two records have been

476 independently dated by means of annual-layer counts in ice cores and U/Th ages of
477 stalagmites. The match suggests that these atmospheric ^{14}C plateaus may largely result
478 from changes in air-sea gas exchange, and in turn, from changes in ocean dynamics.

479

480 In particular, these events may have been linked to a variety of fast changes such as in
481 sea ice cover in the Southern Ocean and/or in the salinity and buoyancy of high-latitude
482 surface waters (Skinner et al., 2010; Burke and Robinson, 2012). These factors control
483 upwelling and meridional overturning of deep waters, in particular found in the Southern
484 Ocean (Chen et al., 2015) and/or North Pacific (Rae et al. 2014, Gebhardt et al., 2008).
485 Such events of changes in MOC geometry and intensity may be responsible for ocean
486 degassing and the ^{14}C plateaus. The enhanced mixing of the Southern Ocean and a
487 similar, slightly later mixing event in the North Pacific (MD02-2489; Fig. S2d) may have
488 triggered – with phase lag – two trends in parallel, (1) a rise in atmospheric CO_2 , in part
489 abrupt (*sensu* Chen et al., 2015; Menviel et al., 2018), and (2) a gradual enrichment in ^{14}C
490 depleted atmospheric carbon, reflected as ^{14}C plateau.

491

492 Plateau 6a matches a ^{14}C plateau deduced from atmospheric ^{10}Be concentrations, thus
493 suggests changes in ^{14}C production. Other changes in atmospheric ^{14}C (plateaus 4 and
494 8) match short-term North Atlantic warmings during peak glacial and earliest deglacial
495 times, similar to that at the end of HS-1 and during plateau 'YD', hence may reflect
496 minor changes in ocean circulation and ocean-atmosphere exchange without major
497 degassing of old ^{14}C depleted deep waters in the North Atlantic (Table 2, Fig. S2a).

498 There is still little information, however, on the origin of several other peak glacial ^{14}C
499 plateaus 17.5–29 cal. ka. The actual linkages of these plateaus to events in ocean MOC
500 still remain to be uncovered.

501

502 3. DISCUSSION and IMPLICATIONS

503 3.1 ^{14}C plateau boundaries – A suite of narrow-spaced age tie points to rate short-term 504 changes in marine sediment budgets, chemical inventories, and climate 29–10 cal. ka

505

506 In continuation of previous efforts (Sarnthein et al., 2007 and 2015) the tuning of high-
507 resolution planktic ^{14}C records of ocean sediment cores to the new age-calibrated
508 atmospheric ^{14}C plateau boundaries now makes it possible to establish a ‘rung ladder’
509 of ~30 age tie points covering the time span 29 – 10 cal. ka. These global tie points
510 have a time resolution of several hundred to thousand years to be used to constrain the
511 chronology and potential leads and lags of events that occurred during peak glacial and
512 deglacial times (Fig. 1). The locations of 18 (20; depending on the age range covered)
513 ^{14}C records are shown in Fig. 7. Figs. 8 and S2 give the time histories of the planktic
514 and benthic reservoir ages, the information they provide is discussed below.

515

516 Six prominent examples showing the power and value of additional information obtained
517 by means of the ^{14}C plateau-tuning method are:

518 (i) The timing of ocean signals of the onset of deglaciation (sudden depletion of
519 planktic $\delta^{18}\text{O}$ and rise in SST) in the North Atlantic and North Pacific can now be
520 distinguished in detail from those in the Southern Hemisphere, where warming began at
521 17.6 cal. ka, when the cooling of Heinrich 1 started in the North Atlantic (Fig. S2)
522 (Küssner et al., 2020 subm.); in harmony with Schmittner and Lund, 2015), a finding
523 important to further constrain global ‘bipolar see-saw’ (Stocker and Johnsen, 2003).

524 (ii) Likewise, the end of the cooling equated with the Antarctic Cold Reversal (ACR;
525 WDC Project Members, 2013) in Pacific surface waters off Central Chile was found

526 precisely coeval with the onset of the Younger Dryas cold spell in the Northern
527 Hemisphere (Küssner et al., 2020 subm.).

528 (iii) Signals of local deep-water formation in the subpolar North Pacific can now be
529 separated from signals originating in the North Atlantic (Rae et al. 2014; Sarnthein et al.,
530 2013). In this way we now can specify and tie major short-lasting reversals in Atlantic
531 and Pacific MOC on a global scale.

532 (iv) Signals of deglacial meltwater advection can now be distinguished from short-
533 term interstadial warmings in the northern subtropical Atlantic, which helps to locate
534 meltwater outbreaks far beyond the well-known Heinrich belt of ice-rafted debris
535 (Balmer and Sarnthein, 2018).

536 (v) As outlined above, the timing of marine ^{14}C plateaus can now be compared in
537 detail with that of deglacial events of climate and the atmospheric CO_2 rise independ-
538 ently dated by means of ice core-based stratigraphy (Table 2; Fig. 6). These linkages
539 offer a tool to explore details of deglacial changes in deep-ocean MOC once the suite of
540 ^{14}C plateaus has been properly tuned at any particular ocean site.

541 (vi) The refined scale of age tie points also reveals unexpected details for changes in
542 the sea ice cover of high latitudes as reflected by anomalously high ^{14}C reservoir ages
543 (e.g. north of Iceland and near to the Azores Islands) and for the evolution of Asian
544 summer monsoon in the northern and southern hemisphere as reflected by periods of
545 reduced sea surface salinity (e.g., Sarnthein et al., 2015; Balmer et al., 2018).

546

547 Finally, the plateau-based high-resolution chronology has led to the detection of
548 numerous millennial-scale hiatuses (e.g., Sarnthein et al., 2015; Balmer et al., 2016;
549 Küssner et al., 2020 subm.) overlooked by conventional, e.g., *AnalySerie*-based
550 methods (Paillard et al. 1996) of stratigraphic correlation (Fig. S2). In turn, the hiatuses

551 give intriguing new insights into past changes of bottom current dynamics linked to
552 different millennial-scale geometries of overturning circulation and climate change such
553 as in the South China Sea (Sarnthein et al., 2013 and 2015), in the South Atlantic
554 (Balmer et al. 2016) and southern South Pacific (Ronge et al., 2019).

555

556 Clearly, the new atmospheric ^{14}C 'rung ladder' of closely-spaced chronostratigraphic tie
557 points has evolved to a valuable tool to uncover functional chains in paleoceanography,
558 that actually have controlled events of climate change over glacial-to-deglacial times.
559 The extension of the age range back to 29 ka allows constraining potential changes in
560 the ocean dynamics expected for Dansgaard Oeschger (DO) events 2, 3, and 4 as
561 compared to those found for DO-1, though pertinent core records are still missing.

562

563 *3.2 Observed vs. model-based ^{14}C reservoir ages that act as tracer of past changes in*
564 *surface ocean dynamics provide incentive for model refinements*

565

566 Radiocarbon plateau tuning of marine sediment sections to the Suigetsu ^{14}C
567 atmospheric master record allows us to establish at semi-millennial-scale resolution the
568 difference between the average ^{14}C age of coeval atmospheric and planktic ^{14}C
569 plateaus. The suite of changing ^{14}C reservoir ages over time forms a prime tracer of
570 past ocean dynamics influencing local surface waters and a data set crucial to deduce
571 past apparent deep-water ventilation ages (e.g., Muglia et al., 2018; Cook and Keigwin,
572 2015; Balmer and Sarnthein, 2018).

573

574 To better constrain the water depth of past reservoir ages we dated monospecific
575 planktic foraminifera (Sarnthein et al., 2007); in low-to-mid latitudes on *G. bulloides*, *G.*

576 *ruber*, or *G. sacculifer* with habitat depths of 0–80/120 m (Jonkers and Kucera, 2017)
577 and in high latitudes, mostly on *N. pachyderma* (s) living at 0–200 m depth (Simstich et
578 al., 2003). Averaging of ^{14}C ages within a ^{14}C plateau helps to remove analytical noise
579 and minor real ^{14}C fluctuations. Nine plateaus are located in the LGM, 18–27 cal. ka
580 (Fig. 1). Here, planktic foraminifera-based reservoir ages show analytical uncertainties
581 of >200 to >300 yr each for standard AMS dating. By comparison, short-term temporal
582 variations in reservoir age reach 200–400 yr, occasionally up to 600 yr, in particular,
583 close to the end of the LGM (Table 3).

584

585 To better decode the informative value of our ^{14}C reservoir ages for late LGM we
586 compared average ages of ^{14}C Plateaus 4-5 (18.6–20.9 cal. ka) with estimates
587 generated by various global ocean models, an approach similar to that of Toggweiler et
588 al. (2019) applied to modern reservoir ages of the global ocean. In an earlier paper
589 (Balmer et al., 2016) we compared our empiric reservoir ages for the LGM with GCM-
590 based estimates of Franke et al. (2008) and Butzin et al. (2012). Franke et al. (2008)
591 underestimated our mid-latitude values by up to ~ 2000 ^{14}C yr, while LGM reservoir age
592 estimates of Butzin et al. (2012) were more consistent with ours. Their GCM
593 considered more realistic boundary conditions such as the LGM freshwater balance in
594 the Southern Ocean and, in particular, LGM SST and wind fields plus the gas transfer
595 velocity for the exchange of ^{14}C of CO_2 (Sweeney et al., 2007). Further improvements
596 are expected from a model configuration that properly resolves the topographic details
597 of the continental margins and adjacent seas, which frequently form the origin of our
598 sediment-based data sets (Butzin et al., 2020). For the time being, we compared our
599 empirical estimates with estimates from a coarse-resolution GCM, using the results by
600 Muglia et al. (2018; 0–50 m w.d.; Fig. 8c-d; Table 3) as an example. Their model

601 includes ocean surface reservoir age and ocean radiocarbon fields that have been
602 validated through a comparison to LGM ^{14}C data compilation made by Skinner et al.
603 2017. It conforms two plausible, recent model estimates of surface reservoir ages that
604 can be compared to our results (Table 3).

605

606 Low LGM values (300–750 yr) supposedly document an intensive exchange of surface
607 waters with atmospheric CO_2 , most common in model- and foraminifera-based
608 estimates of the low- and mid-latitude Atlantic. Low empiric values also mark LGM
609 waters in mid to high latitudes off Norway and off middle Chile, that is, close to sites of
610 potential deep and/or intermediate water formation. Off Norway and in the northeastern
611 Atlantic, model-based reservoir ages of Muglia et al. (2018) largely match the empiric
612 range. However, the uncertainty envelopes for data shown in Fig. 8c (± 560 yr; $r = 0.59$)
613 generally exceed by far the spatial differences calculated for the empiric data.

614 Conversely, model-based reservoir ages reproduce only poorly the low planktic
615 foraminifera-based estimates off Central Chile and values in the Western Pacific and
616 Southern Ocean.

617 In part, the differences may be linked to problems like insufficient spatial resolution
618 along continental margins, ignoring east-west differences within ocean basins, and/or
619 the estimates of a correct location and extent of seasonal sea ice cover used as LGM
620 boundary condition such as east off Greenland, in the subpolar northwest Pacific, and
621 off Southern Chile, where sea ice hindered the exchange of atmospheric carbon (per
622 analogy to that of temperature exchange, e.g., Sessford et al, 2019). Also, model
623 estimates of the annual average are compared to ^{14}C signals of planktic foraminifera
624 that mostly formed during summer only, e.g., when large parts of the Nordic Seas were

625 found ice-free (Sarnthein et al., 2003). Hence, models may need to better constrain
626 local and seasonal sealing effects of LGM sea ice cover.

627

628 In general, the foraminifera-based reservoir age estimates for our sites that represent
629 various hydrographic key regions in the high-latitude ocean appear much higher than
630 model-derived values. These deviations reach up to 1400 yr, in particular in the
631 Southern Ocean. In part, they may result from the fact that present models may not yet
632 be suited to capture small-scale ocean structures such as the interference of ocean
633 currents with local bathymetry and local upwelling cells. Here, model-based reservoir
634 ages appear far too low in LGM regions influenced by regional upwelling such as the
635 South China Sea then governed by an estuarine overturning system (Wang et al., 2005;
636 Fig. 9), by coastal upwelling off N.W. Australia (Xu et al., 2010; Sarnthein et al., 2011),
637 or by a melt water lid such as off eastern New Zealand (Bostock et al., 2013; Küssner et
638 al., 2020 subm.). Local oceanic features are likely to be missed in current resolution
639 models. Our more narrow-spaced empiric data could help to refine the skill of models to
640 capture past ^{14}C reservoir ages.

641

642 Various differences amongst plankton- and model-based reservoir ages may also result
643 from differential seasonal habitats of the different planktic species analyzed that, in turn,
644 may trace different surface and subsurface water currents. Distinct interspecies
645 differences were found in Baja California that record differential, upwelling-controlled
646 habitat conditions (Lindsay et al, 2015). In the northern Norwegian Sea interspecies
647 differences amount up to 600 yr for the Preboreal ^{14}C plateau, 9.6–10.2 cal. ka
648 (Sarnthein and Werner, 2018). Here ^{14}C records of Arctic *Turborotalita quinqueloba*,
649 dominantly grown close to the sea surface during peak summer, differ from the paired

650 record of *Neogloboquadrina pachyderma*, formed in subsurface waters, and that of
651 subpolar species *N. incompta*, mainly advected from the south by Norwegian Current
652 waters well mixed with the atmosphere during peak winter. This makes closer
653 specification of model results as product of different seasonal extremes a further target.

654

655 *3.3 Planktic foraminifera-based ¹⁴C reservoir ages – A prime database to estimate past*
656 *changes in the ¹⁴C ventilation age of deep waters and past oceanic MOC and DIC*

657

658 ‘Raw’ apparent benthic ventilation ages (in ¹⁴C yr; ‘raw’ *sensu* Balmer et al., 2018)
659 express the difference between the (coeval) atmospheric and benthic ¹⁴C levels
660 measured at any site and time of foraminifer deposition. These ages are the sum of (1)
661 the planktic reservoir age of the ¹⁴C plateau that covers a group of paired benthic and
662 planktic ¹⁴C ages and (2) the (positive or negative) ¹⁴C age difference between any
663 benthic ¹⁴C age and the average ¹⁴C age of the paired planktic ¹⁴C plateau. The benthic
664 ventilation ages necessarily rely on the high quality of ¹⁴C plateau-based chronology,
665 since the atmospheric ¹⁴C level has been subject to substantial short-term changes over
666 glacial-to-deglacial times. Necessarily, the ventilation ages include a mixing of different
667 water masses that might originate from different ocean regions and may contribute
668 differential ¹⁴C ventilation ages, an unknown justifying the modifier ‘apparent’.

669

670 In a further step, the $\Delta\Delta^{14}\text{C}$ equivalent of our ‘raw’ benthic ventilation age may be
671 adjusted to changes in atmospheric ¹⁴C that occurred over the (short) time span
672 between deep-water formation and benthic sediment deposition (e.g., Balmer and
673 Sarnthein, 2018; Cook and Keigwin, 2015). In most cases, however, this second step is

674 omitted since its application usually does not imply any major modification of the
675 ventilation age estimates (Fig. S2a; Skinner et al., 2017; Sarnthein et al., 2013).

676

677 On the basis of ^{14}C plateau tuning we now can rely on 18 accurately dated records of
678 apparent benthic ^{14}C ventilation ages (Fig. S2a-d) to reconstruct the global geometry of
679 LGM and HS-1 deep and intermediate water circulation as summarized in ocean
680 transects and maps (Figs. 9–11) and discussed below. The individual matching of our
681 20 planktic ^{14}C plateau sequences with that of the Suigetsu atmospheric ^{14}C record is
682 displayed in Sarnthein et al. (2015), Balmer et al., (2016), Küssner et al. (2020 subm.),
683 and Ausin et al. (in prep.). In addition, robust estimates of past reservoir ages are
684 obtained for 4 planktic and benthic ^{14}C records from paired atmospheric ^{14}C ages of
685 wood chunks (Rafter et al., 2018; Zhao and Keigwin, 2018; Broecker et al., 2004).

686

687 *3.3.1 — Major features of ocean meridional overturning circulation during LGM (Fig. 10)*

688

689 Off Norway and near the Azores Islands very low benthic ^{14}C ventilation ages of <100–
690 750 yr suggest ongoing deep-water formation in the LGM northern North Atlantic
691 reaching down to more than 3000–3500 m water depth, with a flow strength possibly
692 similar to today (and a coeval deep countercurrent of old waters from the Southern
693 Ocean flowing along the East Atlantic continental margin off Portugal). This pattern
694 clearly corroborates the assembled benthic $\delta^{13}\text{C}$ record showing plenty of elevated $\delta^{13}\text{C}$
695 values for the northwestern, eastern and central North Atlantic (Sarnthein et al., 1994;
696 Millo et al., 2006; Keigwin and Swift, 2017). Irrespective of unspecified potential zonal
697 variations in deep-water ventilation age at mid latitudes and different from a number of
698 published models (e.g., Ferrari et al., 2014; Butzin et al., 2017) this ‘anti-estuarine’

699 pattern has been confirmed by MIROC model simulations (Gebbie, 2014; Sherriff-
700 Tadano et al., 2017, Yamamoto et al., 2019) and, independently, by ϵ_{Nd} records (Howe
701 et al., 2016; Lippold et al., 2016). The latter suggest an overturning of AMOC possibly
702 even stronger than today, in particular due to a ‘thermal threshold’ (Abé-Ouchi, pers.
703 comm.) overlooked in other model simulations.

704

705 In contrast to the northern North Atlantic, deep waters in the southern North Atlantic and
706 Circumpolar (CP) deep waters in the subpolar South Atlantic show an LGM ^{14}C
707 ventilation age of ~ 3640 yr, finally rising up to 3800 yr (Figs. 10, 11, S2b). These waters
708 were upwelled and admixed from below to surface waters near to the sub-Antarctic
709 Front during terminal LGM (Fig. S2b; Skinner et al., 2010; Balmer and Sarnthein, 2016;
710 model of Butzin et al., 2012).

711

712 In the southwestern South Pacific abyssal, in part possibly Antarctic-sourced waters
713 (Rae and Broecker, 2018) likewise show high apparent ^{14}C ventilation ages of 3500 yr
714 that drop to 2750 yr near the end of the LGM (Figs. 10 top and S2c) (^{14}C dates of
715 Ronge et al., 2016, modified by planktic ^{14}C reservoir ages of Küssner et al., 2020
716 subm.). A vertical transect of benthic $\delta^{13}\text{C}$ (McCave et al., 2008) suggests that the
717 abyssal waters were overlain by CP waters, separated by pronounced stratification near
718 $\sim 3500\text{--}4000$ m water depth. In part, the CP waters stemmed from North Atlantic Deep
719 Water. Probably, their apparent ventilation age 3500 yr came close to the values found
720 in the southern South Atlantic. East of New Zealand the CP waters entered the deep
721 western Pacific and spread up to the subpolar North Pacific, where LGM ^{14}C ventilation
722 ages reached ~ 3700 yr, possibly occasionally 5000 yr (Fig. S2d).

723

724 Similar to today, the MOC of the LGM Pacific was shaped by estuarine geometry,
725 probably more weakened than today (Du et al., 2018) and more distinct in the far
726 northwest than in the far northeast. This geometry resulted in an upwelling of old deep
727 waters in the subarctic Northwest Pacific, here leading to a ^{14}C reservoir age of ~1700
728 yr for surface waters at terminal LGM. On top of the Lower Pacific Deep Waters we may
729 surmise Upper Pacific Deep Waters that moved toward south (Figs. 10 top and 11).

730

731 The Pacific deep waters were overlain by Antarctic / Pacific Intermediate Waters (IW)
732 with LGM ^{14}C ventilation ages as low as 1400–1800 yr, except for a shelf ice-covered
733 site at the southern tip of Chile with IW ages of 2400–2900 yr, possibly a result of local
734 upwelling of CP waters. In general, however, the low values of Pacific IW are similar to
735 those estimated for South Atlantic IW and likewise reflect a vivid exchange with
736 atmospheric CO_2 in their source regions in the Southern Ocean (Skinner et al., 2015).

737

738 When entering and crossing the entrance sill to the marginal South China Sea the
739 ‘young’ IW were mixed with ‘old’ CP waters entrained from below, here leading to ^{14}C
740 ventilation ages of 2600–3450 yr (Figs. 9 and S2d). The LGM South China Sea was
741 shaped by an estuarine-style overturning system marked by major upwelling near to its
742 distal end in the far southwest (Wang L. et al., 1999). This upwelling led to planktic ^{14}C
743 reservoir ages as high as 1200–1800 yr, values rarely found elsewhere in surface
744 waters of low latitudes.

745

746 Our wide-spaced distribution pattern of 18 open-ocean ^{14}C ventilation ages (plus 4
747 values based on paired wood chunks) in Figs. 10 and 11 agrees only in part with the
748 circulation patterns suggested by the much larger datasets of ^{14}C ventilation ages

749 compiled by Skinner et al. (2017) and Zhao et al. (2018). Several features in Figs. 10
750 and 11 directly deviate, e.g., the ages we derive for the North Atlantic and mid-depth
751 Pacific. These deviations may be linked to both the different derivation of our ^{14}C
752 ventilation age estimates and the details of our calendar-year chronology now based on
753 the narrow-standing suite of ^{14}C plateau-boundary ages. The quality of our ^{14}C reservoir
754 ages of surface waters also controls the 'apparent' ventilation age of deep-waters, as it
755 results from direct addition of the short-term average ^{14}C age of a planktic ^{14}C plateau to
756 a paired, that is coeval benthic ^{14}C age (formed during the time of benthic foraminiferal
757 growth, somewhat after the actual time of deep-water formation).

758

759 *3.3.2 — Major features of meridional overturning circulation during early HS-1 (Fig. 10)*

760

761 Near the onset of deglacial Heinrich Stadial 1 (HS-1; ~18–14.7 cal. ka) major shifts in
762 ^{14}C ventilation age suggest some short-lasting but fundamental changes in the
763 circulation geometry of the deep ocean, a central theme of marine paleoclimate
764 research (lower panel of Figs. 10, 11 and S2a and b). Deep waters in the eastern
765 Nordic Seas, west of the Azores Islands, and off northern Brazil show a rapid rise to
766 high ^{14}C ventilation ages of ~2000–2500 yr and up to 4000 yr off Brazil, values that give
767 first proof for a brief switch from 'anti-estuarine' to 'estuarine' circulation that governed
768 the central North Atlantic and Norwegian Sea during early HS-1. This geometry
769 continued – except for a brief but marked and widespread event of recurring NADW
770 formation near 15.2 ka – until the very end of HS-1 near 14.5 ka (Fig. S2a; Muschitiello
771 et al., 2019). The MOC switch from LGM to HS-1 is in line with changes depicted in
772 paired benthic $\delta^{13}\text{C}$ data (Sarnthein et al., 1994), but not confirmed by the coeval ϵ_{Nd}

773 record that suggests a constant source of 'mid-depth waters', with the $\delta^{13}\text{C}$ drop being
774 simply linked to a higher age (Howe et al., 2018).

775

776 Conversely, benthic ^{14}C ventilation ages in the northeastern North Pacific (Site MD02-
777 2489) show a coeval and distinct but brief minimum of 1050-1450 yr near 3640 m w.d.
778 during early HS-1 (~18.1–16.8 ka; Figs. 10, 11, and S2d). This minimum was produced
779 by extremely small benthic-planktic age differences of 350–650 yr and provides robust
780 evidence for a millennial-scale event of deep-water formation, that has flushed the
781 northeastern North Pacific down to more than 3640 m w.d. (Gebhardt et al., 2008;
782 Sarnthein et al., 2013; Rae et al., 2014). Similar circulation geometries were reported for
783 the Pliocene (Burls et al., 2017). 'Young' Upper North Pacific Deep Waters (North
784 Pacific Intermediate Waters *sensu* Gong et al., 2019) then penetrated as 'western
785 boundary current' far south, up to the northern continental margin of the South China
786 Sea (Figs. 9b, 11, and S2d). The short-lasting North Pacific regime of anti-estuarine
787 overturning was similar to that we find in the modern and LGM Atlantic and, most
788 interesting, simultaneous with the Atlantic's estuarine episode.

789

790 Recent data on benthic-planktic ^{14}C age differences (Du et al., 2018) precisely recover
791 our results in a core at ~680 m w.d. off southern Alaska. However, they do not depict
792 the 'young' deep waters at their Site U1418 at ~3680 m w.d., as corroborated by a
793 paired autigenic ϵ_{Nd} maximum suggesting a high local bottom water age nearby. We
794 assume that the amazing difference in local deep-water ventilation ages is due to small-
795 scale differences in the effect of Coriolis forcing at high latitudes between a site located
796 directly at the base of the Alaskan continental margin (U1418; Fig. 10b) and that on the
797 distal Murray Sea Mount in the 'open' Pacific (MD02-2489; Figs. 7 and 11), which

798 probably has been washed by a plume of newly formed North Pacific deep waters
799 probably stemming from the Bering and/or Ochotsk Seas. In contrast, the incursion of
800 almost 3000 yr old deep waters from the Southern Ocean has continued along the
801 continental margin all over HS-1. In summary we may conclude that the geometry of
802 ocean MOC was briefly reversed in the 'open' North Pacific over almost 1500 years
803 during HS-1, far deeper than suggested by previous authors (e.g., Okazaki et al., 2012;
804 Gong, S., et al. 2019), but similar to changes in geometry first proposed by Broecker et
805 al. (1985) then, however, for an LGM ocean.

806

807 3.3.3 — *Deep-Ocean DIC inventory*

808

809 Apart from the changing geometries in ocean MOC during LGM and HS-1, the global
810 set of ^{14}C plateau-based, hence refined estimates of apparent ^{14}C ventilation ages (Fig.
811 10) has ultimately also revealed new insights into glacial-to-deglacial changes in deep-
812 ocean DIC inventories (Sarnthein et al., 2013; Skinner et al., 2019). On the basis of
813 GLODAP data (Key et al., 2004) any drop in ^{14}C concentration (i.e., any rise in average
814 ^{14}C ventilation age) of modern deep waters is tied linearly to a rise of carbon (DIC)
815 dissolved in deep ocean waters below ~2000 m, making for 1.22 micromole C / -1 ‰
816 ^{14}C . By and large, GCM and box model simulations of Chikamoto and Abé-Ouchi (2012)
817 and Wallmann et al. (2016) suggest that this ratio may also apply to LGM deep-water
818 circulation, when apparent ^{14}C ventilation ages in the Southern Ocean increased
819 significantly (from 2400 up to ~3800 yr) and accordingly, thermohaline circulation was
820 more sluggish and transit times of deep waters extended. Accordingly, a 'back-of-the-
821 envelope' calculation of LGM ventilation age averages in the global deep ocean
822 suggests an additional carbon absorption of 730–980 Gt (Sarnthein et al., 2013). This

823 estimate can easily accommodate the glacial transfer of ~200 Gt C from the atmosphere
824 and biosphere, moreover, may also explain 200–450 Gt C then most probably removed
825 from glacial Atlantic and Pacific intermediate waters. These estimates offer an
826 independent evaluation of ice core-based data, other proxies, and model-based data on
827 past changes in the global carbon cycle (e.g., Menviel et al., 2018).

828

829 4. SOME CONCLUSIONS AND PERSPECTIVES

830 – Despite some analytical scatter, ^{14}C ages for the top and base of Lake Suigetsu-
831 based atmospheric ^{14}C plateaus and coeval planktic ^{14}C plateaus do not present
832 statistical ‘outliers’ but real age estimates that are reproduced by tree ring-based ^{14}C
833 ages over the interval 10–13 cal. ka and further back.

834 – Hulu U/Th model-based ages of ^{14}C plateau boundaries of the Suigetsu atmospheric
835 ^{14}C record appear superior to those derived from microscopy-based varve counts only,
836 since U/Th model-based ages match far more closely the age when now deduced from
837 XRF-based varve counts for the tie point of lower plateau boundary 2b, a test case in
838 the early deglacial, and for the age assigned to the Laschamp event prior to the LGM.

839 – During deglacial times, we show that several atmospheric ^{14}C plateaus paralleled a
840 rise in air-sea gas exchange, and, in turn, distinct changes in ocean MOC. Changes in
841 cosmogenic ^{14}C production rarely provide a complete explanation for the plateaus
842 identified in the Suigetsu ^{14}C data under discussion.

843 – In total, ^{14}C plateau boundaries in the range now provide a suite of ~30 age tie points
844 to establish – like chronological ladder rungs – a robust global age control for deep-sea
845 sediment sections and global stratigraphic correlations of last glacial to deglacial climate
846 events, 29–10 cal. ka. U/Th model ages confine the cal. age uncertainty of Suigetsu
847 plateau boundaries assigned halfway between two ^{14}C ages nearby inside and outside

848 a plateau's scatter band to less than ± 50 to ± 70 yr. Nevertheless, stratigraphic gaps
849 may hamper the accurate tuning of planktic ^{14}C plateaus to their atmospheric
850 equivalents hence result in major discrepancies.

851 – The difference in ^{14}C age between coeval atmospheric and planktic ^{14}C plateaus
852 presents a robust tracer of planktic ^{14}C reservoir ages and shows their high temporal
853 and spatial variability for the LGM and HS-1, now established for 18/20 sediment sites.

854 – Paired reservoir ages obtained from different planktic species document the local
855 distribution patterns of different surface water masses and prevailing foraminiferal
856 habitats at different seasons yet insufficiently considered in model simulations.

857 – New, more robust deep-water ^{14}C ventilation ages, derived on the basis of our robust
858 planktic ^{14}C reservoir ages, reveal geometries of LGM overturning circulation similar to
859 those of today. In contrast, ^{14}C ventilation ages of early HS-1 suggest an almost 1500 yr
860 long event of widely reversed circulation patterns marked by deep-water formation and
861 brief flushing of the northern North Pacific and estuarine circulation geometry in the
862 northern North Atlantic.

863 – Increased glacial ^{14}C ventilation ages and carbon (DIC) inventories of ocean deep
864 waters suggest an LGM drawdown of about 850 Gt C into the deep ocean. Starting with
865 HS-1 a drop of ventilation age suggests carbon released to the atmosphere (Sarnthein
866 et al., 2013).

867 – Site-specific comparison of planktic and model-based reservoir ages estimates
868 highlights the need for further model refinements to make them better reflect the real
869 complex patterns of ocean circulation, including seasonality.

870

871 ACKNOWLEDGMENTS

872 We owe sincere thanks for plenty of stimulations to the 23rd International Radiocarbon
873 Conference in Trondheim, in particular to M-J. Nadeau, and to the IPODS–OC3
874 workshop in Cambridge U.K, 2018, convened by A. Schmittner and L. Skinner.
875 Moreover, we thank for most valuable basic discussions with R. Staff, Glasgow, J.
876 Southon, Irvine CA, and M. Butzin, AWI Bremerhaven, who kindly helped us to discuss
877 the comparison of his model results, and S. Beil, Kiel, for computer assistance. Over the
878 last three years, G. Mollenhauer measured with care hundreds of supplementary ¹⁴C
879 ages in her MICADAS laboratory at AWI Bremerhaven. This study obtained long lasting
880 special support from R. Tiedemann and his colleagues at the AWI Bremerhaven.

881

882 **Author contribution**

883 All authors contributed data and valuable suggestions to write up this synthesis. MS and
884 PG designed the outline of this manuscript. KK, BA, TE and MS provided new marine
885 ¹⁴C records in addition to records previously published. GS displayed the details of
886 Suigetsu varve counts. RM provided a ¹⁰Be-based ¹⁴C record and plots of raw ¹⁴C data
887 sets of Suigetsu und Hulu Cave. Discussions amongst PG, RM, GS and MS served to
888 select U/Th-based model ages as best-possible time scale. JM streamlined the sections
889 on data-model intercomparison.

890

891 **Data availability**

892 **Published primary radiocarbon data of all sites are available at PANGAEA de. ¹⁴C data**
893 **of 5 marine cores still under publication by Küssner et al. (2020 subm.) and Ausin et al.**
894 **(subm.; also see caption of Fig. S2) are deposited at PANGAEA.**

895

896 REFERENCES (99)

897 Adkins, J. F. and Boyle, E. A.: Changing atmospheric $\Delta^{14}\text{C}$ and the record of
898 paleoventilation ages. *Paleoceanography*, 12(3), 337–344, 1997.

899 Adolphi, F., Bronk Ramsey, C., Erhard, T., Lawrence Edwards, R., Cheng, H.,
900 Turney, C.S.M., Cooper, A., Svensson, A., Rasmussen, S.O., Fischer, H., and

901 Muscheler, R.: Connecting the Greenland ice-core and U/Th timescales via cosmogenic
902 radionuclides: testing the synchronicity of Dansgaard–Oeschger events. *Clim. Past*, 14,
903 1755–1781. <https://doi.org/10.5194/cp-14-1755-2018>, 2018.

904 Alves, E.Q., Macario, K., Ascough, P., and Bronk Ramsey, C.: The worldwide
905 marine radiocarbon reservoir effect: definitions, mechanisms, and prospects. *Review of*
906 *Geophysics*, 56, <https://doi.org/10.1002/2017RG000588>, 2018.

907 Alveson, E.Q.: Radiocarbon in the Ocean, *EOS*, 99,
908 <https://doi.org/10.1029/2018EO095429>, 2018.

909 Ausin, B., Haghpor, N., Wacker, L., Voelker, A. H. L., Hodell, D., Magill, C., et al.:
910 Radiocarbon age offsets between two surface dwelling planktonic foraminifera species
911 during abrupt climate events in the SW Iberian margin. *Paleoceanography and*
912 *Paleoclimatology*, 34. <https://doi.org/10.1029/2018PA003490>, 2019.

913 Balmer, S., Sarnthein, M., Mudelsee, M., and Grootes, P. M.: Refined modeling and
914 ^{14}C plateau tuning reveal consistent patterns of glacial and deglacial ^{14}C reservoir ages
915 of surface waters in low-latitude Atlantic. *Paleoceanography*, 31.
916 <https://doi.org/10.1002/2016PA002953>, 2016.

917 Balmer, S. and Sarnthein, M.: Planktic ^{14}C plateaus, a result of short-term
918 sedimentation pulses? – *Radiocarbon*, 58, DOI:10.1017/RDC.2016.100, 11 pp., 2016.

919 Balmer, S. and Sarnthein, M.: Glacial-to deglacial changes in North Atlantic melt-
920 water advection and deep-water formation – Centennial-to-millennial-scale ^{14}C records
921 from the Azores Plateau. *Geochim. Cosmochim. Acta*, 236, 399-415,
922 <https://doi.org/10.1016/j.gca.2018.03.001>, 2018.

923 Berger W.H. and Keir, R.S.: Glacial-Holocene changes in atmospheric CO_2 and the
924 deep-sea record. J.E. Hansen, T. Takahashi (Eds.), *Geophysical Monograph*, 29,
925 American Geophysical Union, Washington, DC, pp. 337–351, 1984.

926 Bostock, H.C., Barrows, T.T., Carter, L., Chase, Z., Cortese, G., et al.: A review of
927 the Australian – New Zealand sector of the Southern Ocean over the last 30 ka (Aus-
928 INTIMATE project). *Quaternary Science Reviews* 74, 35-57, 2013.

929 Broecker W.S, Peteet, D.M., and Rind, D.: Does the ocean-atmosphere system have
930 more than one stable mode of operation? *Nature*, **315**, 21-26, doi:10.1038/315021a0,
931 1985

932 Broecker W.S., Barker, S., Clark, E., Hajdas, I., Bonani, G., and Stott, L.: Ventilation
933 of the Glacial deep Pacific Ocean, *Science*, 306, 1169–1172, 2004.

934 Bronk Ramsey, C., Staff, R. A., Bryant, C. L., Brock, F., Kitagawa, H., van der Plicht,

935 J., Schlolaut, G., Marshall, M. H., Brauer, A., Lamb, H. F., Payne, R. L., Tarasov, P. E.,
936 Haraguchi, T., Gotanda, K., Yonenobu, H., Yokoyama, Y., Tada, R., and Nakagawa, T.:
937 A complete terrestrial radiocarbon record for 11.2 to 52.8 kyr B.P., *Science*, 338, 370–
938 374, 2012.

939 Bronk Ramsey, C. et al., *Radiocarbon*, (in press) 2020.

940 Burke, A. and Robinson, L.F.: The Southern Ocean's role in carbon exchange during
941 the last deglaciation. *Science*, 335, 557-561, 2012.

942 Burls, N.J., Fedorov, A.V., Sigman, D.M., Jaccard, S.L., Tiedemann, R., and Haug,
943 G.H.: Active Pacific meridional overturning circulation (PMOC) during the warm
944 Pliocene. *Sci. Adv.* 2017;3: e1700156, 2017.

945 Butzin, M., Prange, M., Lohmann, G.: Radiocarbon simulations for the glacial ocean:
946 The effects of wind stress, Southern Ocean sea ice and Heinrich events. *Earth Planet.*
947 *Sci. Lett.*, 235, 45-61, 2005.

948 Butzin, M., Prange, M., and Lohmann, G.: Readjustment of glacial radiocarbon
949 chronologies by self-consistent three-dimensional ocean circulation modeling. *Earth*
950 *Planet Sci. Lett.*, 317, 177-184, 2012.

951 Butzin, M., Köhler, P., and Lohmann, G.: Marine radiocarbon reservoir age
952 simulations for the past 50,000 years. *Geophys. Res. Lett.*, 44, 8473–8480,
953 doi:10.1002/2017GL074688, 2017.

954 Butzin, M., Heaton, T.J., Köhler, P., and Lohmann, G.: A short note on marine
955 reservoir age simulations used in INTCAL20. *Radiocarbon*, oo, 1-7, DOI:10.1017/RDC.2020.9,
956 2020.

957 Chen, T., Robinson, L.F., Burke, A., Southon, J., Spooner, P., Morris, P.J., and Ng,
958 H.C.: Synchronous centennial abrupt events in the ocean and atmosphere during the
959 last deglaciation, *Science*, 349, 1537-1541, 2015.

960 Cheng, H., Edwards, R.L., Southon, J., Matsumoto, K., Feinberg, J.M., Sinha, A.,
961 Zhou, W., Li, H., Li, X., Xu, Y., Chen, S., Tan, M., Wang, Q., Wang, Y., and Ning, Y.:
962 Atmospheric $^{14}\text{C}/^{12}\text{C}$ changes during the last glacial period from Hulu Cave, *Science*,
963 362, 1293-1297, 2018.

964 Chikamoto, M.O., Abé-Ouchi, A., Oka, A., Ohgaito, R., and Timmermann, A.:
965 Quantifying the ocean's role in glacial CO_2 reductions, *Climate of the Past*, 8, 545–563,
966 doi:10.5194/cp-8-545-2012, 2012.

967 Cook M.S. and Keigwin L.D.: Radiocarbon profiles of the NW Pacific from the LGM
968 and deglaciation: Evaluating ventilation metrics and the effect of uncertain surface

969 reservoir ages, *Paleoceanography*, 30, 174–195, 2015.

970 Davies, S.M., Davies, P.M., Abbott, Meara, R.H., et al.: A North Atlantic tephro-
971 stratigraphical framework for 130-60 ka b2k: New tephra discoveries, marine based
972 correlations, and future challenges, *Quaternary Science Rev.*, 106, 101-121, 2014.

973 Du, J., Haley, B.A., Mix, A.C., Walczak, M.H., and Praetorius, S.K.: Flushing of the
974 deep Pacific Ocean and the deglacial rise of atmospheric CO₂ concentrations, *Nature*
975 *geoscience*, 11, 749-755, 2018.

976 Ferrari, R., Jansen, M.F., Adkins, J.F., Burke, A., Stewart, A.L., and Thompson, A.F.:
977 Antarctic sea ice control on ocean circulation in present and glacial climates, *Proc.*
978 *National Academy Science*, 111 (24), 8753–8758, 2014.

979 Gebbie, G.: How much did Glacial North Atlantic Water shoal? *Paleoceanography*,
980 29, 190-209, doi:10.1002/2013PA002557, 2014.

981 Gebhardt, H., Sarnthein, M., Kiefer, T., Erlenkeuser, H., Schmieder, F., and Röhl, U.:
982 Paleonutrient and productivity records from the subarctic North Pacific for Pleistocene
983 glacial terminations I to V. *Paleoceanography* 23, PA4212, 1-21,
984 doi:10.1029/2007PA001513, 2008.

985 Gong, S., Lembke-Jene, L., Lohmann, G., Knorr, G., Tiedemann, R., Zou, J.J and
986 Shi, X.F.: Enhanced North Pacific deep-ocean stratification by stronger intermediate
987 water formation during Heinrich Stadial 1. *Nature Communications*, 10: 656.
988 <https://doi.org/10.1038/s41467-019-08606-2>, 2019.

989 Grootes P.M. and Stuiver, M.: Oxygen 18/16 variability in Greenland snow and ice
990 with 1000 to 100000 year time resolution, *J. Geophys. Res.: Oceans* (1978–2012)
991 102(C12), 26455–26470, 1997.

992 Grootes, P.M. and Sarnthein, M.: Marine ¹⁴C reservoir ages oscillate, *PAGES News*,
993 14/3, 18-19, 2006.

994 Hain, M.P., Sigman, D.M., and Haug, G.H.: Distinct roles of the Southern Ocean and
995 North Atlantic in the deglacial atmospheric radiocarbon decline, *Earth Planetary Science*
996 *Letters* 394, 198-208, 2014.

997 Howe, J.N.W., Piotrowski, A.M., Noble, T.L., Mulitza, S., Chiessi, C.M., and Bayon,
998 G.: North Atlantic deep-water production during the last glacial maximum, *Nat.*
999 *Commun.*, 7, 11765, 2016. s

1000 Howe, J.N.W., Huang, K-F., Oppo, D.W., Chiessi, C.M., Mulitza, S., Blusztajn, J.,
1001 and Piotrowski, A.M.: Similar mid-depth Atlantic water mass provenance during the Last
1002 Glacial Maximum and Heinrich Stadial 1, *Earth Planetary Science Letters*, 490, 51-61,

1003 2018.

1004 Jonkers, L. and Kucera, M.: Quantifying the effect of seasonal and vertical habitat
1005 tracking on planktonic foraminifera proxies, *Climate of the Past*, 13, 573-586, 2017.

1006 Keigwin, L.D. and Swift, S.A.: Carbon isotope evidence for a northern source of
1007 deep water in the glacial western North Atlantic, *PNAS*, 114 (11), 2831-2835, 2017.

1008 Key R. M., Kozyr, A., Sabine, C.L., Lee, K., Wanninkhof, R., Bullister, J.L., Feely,
1009 R.A., Millero, F.J., Mordy, C., and Peng, T.-H. (2004) A global ocean carbon climat-
1010 ology: Results from Global Data Analysis Project (GLODAP), *Global Biogeochem. Cy.*,
1011 18, GB4031, doi:10.1029/2004GB002247, 2004.

1012 Kong, X., Wang, Y., Wu, J., Cheng, H., Edwards, R.L., and Wang, X.: Complicated
1013 responses of stalagmite $\delta^{13}\text{C}$ to climate change during the last glaciation from Hulu
1014 Cave, Nanjing, China, *Science in China Ser. D Earth Sciences*, 48, (12), 2174-2181,
1015 2005.

1016 Küssner, K., Sarnthein, M., Lamy, F., and Tiedemann, R.: High-resolution
1017 radiocarbon-based age records trace episodes of *Zoophycos* burrowing, *Marine*
1018 *Geology*, 403, 48-56, <http://doi:10.1016/j.margeo.2018.04.01>, 2018.

1019 Küssner, K., Sarnthein, M., Lamy, F., Michel, E., Mollenhauer, G., Siani G., and
1020 Tiedemann, R.: Glacial-to-deglacial reservoir ages of surface waters in the southern
1021 South Pacific, *Paleoc. and Paleoclim.* 30 ms-pp, subm.).

1022 Lascu, I., Feinberg, J.M., Dorale, J.A., Cheng, H., and Edwards, R.L.: Age of the
1023 Laschamp excursion determined by U-Th dating of a speleothem geomagnetic record
1024 from North America. *Geology*, 44, 139-142, doi:10.1130/G37490.1. 2016

1025 Lindsay, C.M., Lehman, S.J., Marchitto, T.M., and Ortiz, J.D.: The surface
1026 expression of radiocarbon anomalies near Baja California during deglaciation. *Earth*
1027 *Planetary Science Letters*, 422, 67-74, 2015.

1028 Lippold, J., Gutjahr, M., Blaser, P., Christner, E., de Cavalho-Fereira, M.L., Mulitza,
1029 S. et al.: Deep-water provenance and dynamics of the (de)glacial Atlantic meridional
1030 overturning circulation, *Earth Planetary Science Letters*, 445, 68-78, 2016.

1031 Lisiecki, L.E. and Stern, J.V.: Regional and global benthic $d^{18}\text{O}$ stacks for the last
1032 glacial cycle. *Paleoceanography*, 31, doi:10.1002/2016PA003002, 2016.

1033 Löwemark, L. and Grootes, P.M.: Large age differences between planktic
1034 foraminifers caused by abundance variations and *Zoophycos* bioturbation,
1035 *Paleoceanography*, 19, PA2001, doi:10.1029/2003PA000949, 2004.

1036 Marcott, S.A., Bauska, T.K., Buizert, C., Steig, E.J., Rosen, J.L., Cuffey, K.M.,

1037 Fudge, T.J., Severinghaus, J.P., Ahn, J., Kalk, M.L., McConnell, J.R., Sowers, T.,
1038 Taylor, K.C., White, J.W.C., and Brook, E.J.: Centennial-scale changes in the global
1039 carbon cycle during the last deglaciation, *Nature*, 514, 616-619,
1040 doi:10.1038/nature13799, 2014.

1041 Marshall, M., Schlolaut, G., Brauer, A., Nakagawa, T., Staff, R.A., Bronk Ramsey,
1042 C., Lamb, H., Gotanda, K., Haraguchi, T., Yokoyama, Y., Yonenobu, H., Tada, R.,
1043 SG06 project members: A novel approach to varve counting using μ XRF and X-
1044 radiography in combination with thin-section microscopy, applied to the Late Glacial
1045 chronology from Lake Suigetsu, Japan, *Quaternary Geochronology* 13, 70-80, 2012.

1046 McCave, I.N., Carter, I., and Hall, I.R.: Glacial-interglacial changes in water mass
1047 structure and flow in the SW Pacific Ocean, *Quaternary Science Rev.*, 27, 1886–1908,
1048 2008.

1049 Matsumoto, K.: Radiocarbon-based circulation age of the world oceans, *J. Geophys.*
1050 *Res.: Oceans* 112(C9), C09004. <https://doi.org/10.1029/2007JC004095>, 2007.

1051 Menviel, L., Spence, P., Yu, J., Chamberlain, M.A., Matear, R.J., Meissner K.J., and
1052 England, M.H.: Southern Hemisphere westerlies as a driver of the early deglacial
1053 atmospheric CO₂ rise, *Nature communications*, 9:2503, DOI:10.1038/s41467-018-
1054 04876-4, 2018.

1055 Millo, C., Sarnthein, M., and Erlenkeuser, M.: Variability of the Denmark Strait
1056 Overflow during the Last Glacial Maximum, *Boreas*, 35, 50-60, 2006.

1057 Muglia, J., Skinner, L., and Schmittner, A.: Weak overturning circulation and high
1058 Southern Ocean nutrient utilization maximized glacial ocean carbon, *Earth and*
1059 *Planetary Science Letters* 496, 47-56, 2018.

1060 Muschitiello, F., D'Andrea, W.J., Schmittner, A., Heaton, T.J., Balascio, N.L.,
1061 deRoberts, N., Caffee, M.W., Woodruff, T.E., Welten, K.C., Skinner, L.C., Simon, M.H.,
1062 and Dokken T.M.: Deep-water circulation changes lead North Atlantic climate during
1063 deglaciation, *Nature Communications* 10, 1272, doi.org/10.1038/s41467-019-09237-3,
1064 2019.

1065 Naughton, F., Costas, S., Gomes, S.D., Desprat, S., Rodrigues, T., Sanchez Goñi,
1066 M.F., Renssen, H., Trigo, R., Bronk-Ramsey, C., Oliveira, D., Salgueiro, E., Voelker,
1067 A.H.L., and Abrantes, F.: Coupled ocean and atmospheric changes during Greenland
1068 stadial 1 in southwestern Europe, *Quaternary Science Reviews*, 212, 108-120, 2019.

1069 Nydal R., Lovseth K., and Skogseth F. H.: Transfer of bomb ¹⁴C to the ocean
1070 surface, *Radiocarbon* 22(3), 626–635, 1980.

1071 Okazaki, Y., Sagawa, T., Asahi, H., Horikawa, K., and Onodera, J.: Ventilation
1072 changes in the western North Pacific since the last glacial period, *Climate of the Past*, 8,
1073 17-24, doi:10.5194/cp-8-17-2012, 2012.

1074 Paillard, D., Labeyrie, L., and Yiou, P.: Macintosh program performs time-series
1075 analysis, *Eos Trans, AGU*, **77**: 379, 1996.

1076 Rae, J.W.B. and W. Broecker, W.: What fraction of the Pacific and Indian oceans'
1077 deep water is formed in the Southern Ocean? *Biogeosciences*, 15, 3779-3794, 2018.

1078 Rae, J., Sarnthein, M., Foster, G., Ridgwell, A., Grootes, P.M., and Elliott T.: Deep
1079 water formation in the North Pacific and deglacial CO₂ rise, *Paleoceanography*, 29,
1080 doi:10.1002/2013PA002570, 645–667, 2014.

1081 Rafter, P.A., Herguera, J.-C., and Southon, J.R.: Extreme lowering of deglacial
1082 seawater radiocarbon recorded by both epifaunal and infaunal benthic foraminifera in a
1083 wood-dated sediment core, *Climate of the Past* 14, 1977–1989, 2018.

1084 Reimer P.J., Bard, E., Bayliss, A., Beck, J. W., Blackwell, P.G., Bronk Ramsey, C.,
1085 Buck, C.E., Cheng, H., Edwards, R.L., and Friedrich, M.: IntCal13 and Marine13
1086 radiocarbon age calibration curves 0–50,000 years cal. BP, *Radiocarbon* 55, 1869–
1087 1887, 2013.

1088 Reimer, P.J., et al.: The IntCal 20 northern hemisphere radiocarbon calibration curve
1089 (0-55 kcal BP), *Radiocarbon*, 2020 (in press).

1090 Robinson, L.F., Adkins, J.F., Keigwin, L.D., et al.: Radiocarbon variability in the
1091 western North Atlantic during the last deglaciation, *Science*, 310, 1469-1473, 2005.

1092 Ronge, T. A., Tiedemann, R., Lamy, F., et al.: Radiocarbon constraints on the extent
1093 and evolution of the South Pacific glacial carbon pool, *Nature Comm.* 7:11487, 2016.

1094 Ronge, T.A., Sarnthein, M., Roberts, J., Lamy, F., and Tiedemann, R.: East Pacific
1095 Core PS75/059-2: Glacial-to-deglacial stratigraphy revisited, *Paleoceanography and*
1096 *Paleoclimatology*, 34 (4), 432-435, DOI:10.1029/2019PA003569, 2019.

1097 Sarnthein, M., Winn, K., Jung, S.J., Duplessy, J.C., Labeyrie, L., Erlenkeuser, H.,
1098 and Ganssen, G.: Changes in east Atlantic deepwater circulation over the last 30,000
1099 years: eight time slice reconstructions, *Paleoceanography*, 9(2), 209–267, 1994.

1100 Sarnthein, M., Pflaumann, U., and Weinelt, M.: Past extent of sea ice in the northern
1101 North Atlantic inferred from foraminiferal paleotemperature estimates,
1102 *Paleoceanography*, 18(2), 2003.

1103 Sarnthein, M., Grootes, P.M., Kennett, J.P., and Nadeau, M.: ¹⁴C Reservoir ages
1104 show deglacial changes in ocean currents and carbon cycle, *Geophys. Monograph* –

1105 Am. Geophys. Union, 173, 175–196, 2007.

1106 Sarnthein, M., Grootes, P.M., Holbourn, A., Kuhnt, W., and Kühn, H.: Tropical
1107 warming in the Timor Sea led deglacial Antarctic warming and almost coeval
1108 atmospheric CO₂ rise by >500 yr, *Earth Planetary Science Letters*, 302, 337-348, 2011.

1109 Sarnthein, M., Schneider, B., and Grootes, P.M.: Peak glacial 14C ventilation ages
1110 suggest major draw-down of carbon into the abyssal ocean, *Climate of the Past*, 9 (1),
1111 925–965, 2013.

1112 Sarnthein, M., Balmer, S., Grootes, P.M., and Mudelsee, M.: Planktic and benthic
1113 14C reservoir ages for three ocean basins, calibrated by a suite of 14C plateaus in the
1114 glacial-to-deglacial Suigetsu atmospheric 14C record, *Radiocarbon*, 57, 129–151, 2015.

1115 Sarnthein, M. and Werner, K.: Early Holocene planktic foraminifers record species-
1116 specific ¹⁴C reservoir ages in Arctic Gateway, *Marine Micropaleontology*, 135, 45-55.
1117 DOI:10.1016/j.marmicro.2017.07.002, 2018.

1118 Schlolaut, G.: A unique and easy-to-use-tool to deal with incompletely varved
1119 archives 782 – the Varve Interpolation Program 3.0.0, *Quaternary Geochronology*, 2019
1120 (in press).

1121 Schlolaut, G., Staff, R.A., Marshall, M.H., Brauer, A., Bronk Ramsey, C., Lamb, H.F.,
1122 and Nakagawa, T.: Microfacies analysis of the Lake Suigetsu (Japan) sediments from
1123 ~50 to ~10 ka BP and an extended and revised varve based chronology, *Quaternary
1124 Science Reviews*, 200, 351-366, 2018.

1125 Schmittner, A. and Lund, D.C.: Early deglacial Atlantic overturning decline and its
1126 role in atmospheric CO₂ rise inferred from carbon isotopes ($\delta^{13}\text{C}$), *Climate of the Past*,
1127 11, 135-152, 2015.

1128 Schroeder, J., Holbourn, A., Küssner, K., and Kuhnt, W.: Hydrological variability in
1129 the southern Makassar Strait during the last glacial termination, *Quaternary Science
1130 Reviews*, 154, 143-156, 2016.

1131 Sessford, E.G., Jensen, M.F., Tisserand, A.A., Muschitiello, F., Dokken, T.,
1132 Nisancioglu, K.H., and Jansen, E.: Consistent fluctuations on intermediate water
1133 temperature off the coast off Greenland and Norway during Dansgaard-Oeschger
1134 events, *Quaternary Science Reviews*, 223, 105887, 1-17, 2019.

1135 Sherriff-Tadano, S., Abe-Ouchi, A., Yoshimori, M., Oka, A., and Chan, W.-L.:
1136 (Influence of glacial ice sheets on the Atlantic meridional overturning circulation through
1137 surface wind change, *Climate Dynamics*, 50 (7-8), 2881–2903, 2017.

1138 Siani, G., Michel, E., De Pol-Holz, R., DeVries, T., Lamy, F., Carel, M., Isguder, G.,
1139 Dewilde, F., Lourantou, A.: Carbon isotope records reveal precise timing of enhanced
1140 Southern Ocean upwelling during the last deglaciation, *Nature Communications*, 4,
1141 2758, 2013.

1142 Sikes, E.L. and Guilderson, T.P.: Southwest Pacific Ocean surface reservoir ages
1143 since the last deglaciation: Circulation insights from multiple-core studies. *Paleocean-*
1144 *ography*, 31, 298–310, doi:10.1002/2015PA002855, 2016.

1145 Simstich, J., Sarnthein, M., and Erlenkeuser, H.: Paired $\delta^{18}\text{O}$ signals of
1146 *Neogloboquadrina pachyderma* (s) and *Turborotalita quinqueloba* show thermal
1147 stratification structure in Nordic Seas, *Mar. Micropaleontol.*, 912, 1–19, 2003.

1148 Skinner, L.C., Fallon, S., Waelbroeck, C., Michel, E., and Barker, S.: Ventilation of
1149 the deep Southern Ocean and deglacial CO₂ rise, *Science*, 328, 1147–1151, 2010.

1150 Skinner, L.C., Waelbroeck, C., Scrivner, A.E., and Fallon, S.J.: Radiocarbon
1151 evidence for alternating northern and southern sources of ventilation of the deep
1152 Atlantic carbon pool during the last deglaciation, *PNAS*, 111, 5480–5484, 2014.

1153 Skinner, L.C. *et al.*: Reduced ventilation and enhanced magnitude of the deep
1154 Pacific carbon pool during the last glacial period, *Earth Planetary Science Letters*, **411**,
1155 45-52, 2015.

1156 Skinner, L.C., Primeau, F., Freeman, E., de la Fuente, M., Goodwin, P.A.,
1157 Gottschalk, J., Huang, E., McCave, I.N., Noble, T.L., and Scrivner A.E.: Radiocarbon
1158 constraints on the glacial ocean circulation and its impact on atmospheric CO₂, *Nature*
1159 *communications*, 8:16010, DOI: 10.1038/ncomms16010, 2017.

1160 Skinner, L.C., Muschitiello, F., and Scrivner, A.E.: Marine reservoir age variability
1161 over the last deglaciation: Implications for marine carbon cycling and prospects for
1162 regional radiocarbon calibrations. *Paleoceanography and Paleoclimate*, 34,
1163 doi.org/10.1029/2019PA003667, 2019.

1164 Southon, J., Noronha, A.L., Cheng, H, Edwards, R.L., and Wang, Y.: A high-
1165 resolution record of atmospheric ¹⁴C based on Hulu Cave speleothem H82, *Quaternary*
1166 *Science Reviews*, 33:32-41, 2012.

1167 Steffensen, J.P., Andersen, K.K., Bigler, M., et al.: High-Resolution Greenland Ice
1168 Core Data Show Abrupt Climate Change Happens in Few Years, *Science*, 321, 680;
1169 DOI: 10.1126/science.1157707, 2008.

1170 Stern, J.V. and Lisiecki, L.E.: North Atlantic circulation and reservoir age changes
1171 over the past 41,000 years, *Geophysical Research Letters*, 40, 3693-3697,
1172 doi:10.1002/grl.5067, 2013.

1173 Stocker, T. and Johnsen, S.J.: A minimum thermodynamic model for the bipolar
1174 seesaw, *Paleoceanography*, 18 (4), 1087, doi:10.1029/2003PA000920, 2003.

1175 Stuiver, M. and Braziunas, T.V.: Modeling atmospheric ¹⁴C influences and ¹⁴C ages
1176 of marine samples to 10,000 B.C., *Radiocarbon*, 35, 137–189, 1993.

1177 Svensson, A., Andersen, K.K., Bigler, M., Clausen, H.B., Dahl-Jensen, D., Davies,
1178 S.M., Johnsen, S.J., Muscheler, R., Parrenin, F., Rasmussen, S.O., Röthlisberger, R.,
1179 Seierstad, I., Steffensen, J.P., and Vinther, B.M.: A 60 000 year Greenland stratigraphic
1180 ice core chronology, *Climate of the Past*, 4, 47–57, 2008.

1181 Toggweiler, J.R., Druffel, E.R.M., Key, R.M., and Galbraith, E.D.: Upwelling in the
1182 ocean basins north of the ACC. Part 2: How cool Subantarctic water reaches the
1183 surface in the tropics, *J. Geophysical Research*, DOI:[10.1029/2018JC014795](https://doi.org/10.1029/2018JC014795), 2019 (in
1184 press).

1185 Turney, C.S.M., Fifield, L.K., Hogg, A.G., et al.: Using New Zealand kauri (*Agathis*
1186 *australis*) to test the synchronicity of abrupt climate change during the Last Glacial
1187 Interval (60,000–11,700 years ago), *Quatern. Sci. Rev.*, 29, 3677–3682, 2010.

1188 Turney, C.S.M., Jones, R.T., Phipps, S.J., et al.: Rapid global ocean-atmosphere
1189 response to Southern Ocean freshening during the last glacial, *Nature communications*,
1190 8:520, doi:10.1038/s41467-017-00577-6, 2017.

1191 Umling, N.E. and Thunell, R.C.: Synchronous deglacial thermocline and deep-
1192 water ventilation in the eastern equatorial Pacific, *Nature communications*, 8, 14203.
1193 DOI: 10.1038/ncomms14203, 2017.

1194 Waelbroeck, C., Duplessy, J.-C., Michel, E., Labeyrie, L., Paillard, D., and Duprat, J.:
1195 The timing of the last deglaciation in North Atlantic climate records, *Nature*, 412, 724–
1196 727, 2001.

1197 Waelbroeck, C., Skinner, L.C., Labeyrie, L., Duplessy, J.-C., Michel, E., Riveiros,
1198 N.V., Gherardi, J.-M., and Dewilde, F.: The timing of deglacial circulation changes in the
1199 Atlantic, *Paleoceanography*, 26, PA3213, <https://doi.org/10.1029/2010PA002007>, 2011.

1200 Wallmann, K., Schneider, B., and Sarthein, M.: Effects of eustatic sea-level
1201 change, ocean dynamics, and nutrient utilization on atmospheric pCO₂ and seawater
1202 composition over the last 130,000 years – a model study, *Climate of the Past*, 12, 339-
1203 375, doi: 10.5194/cp-12-339-2016, 2016.

1204 Wang Y.C, Cheng, H., Edwards, R.L., An, Z.S., Wu, J.Y., Shen, C.-C., and Dorale,
1205 J.A.: A high-resolution absolute-dated Late Pleistocene monsoon record from Hulu
1206 Cave, China, *Science*, 294, 2345-2348. DOI: 10.1126/science.1064618, 2001.

1207 Wang, L.J., Sarnthein, M., Erlenkeuser, H., Grimalt, J., Grootes, P., Heilig, S.,
1208 Ivanova, E., Kienast, M., Pelejero, C., and Pflaumann, U.: East Asian monsoon climate
1209 during the late Pleistocene: High-resolution sediment records from the South China
1210 Sea, *Marine Geology*, 156, 245-284, 1999.

1211 Wang, P., Clemens, S., Beaufort, L., Braconnot, P., Ganssen, G., Jian, Z., Kershaw,
1212 P., and Sarnthein, M.: SCOR/IMAGES Working Group 113 SEAMONS: Evolution and
1213 variability of the Asian Monsoon System: State of the art and outstanding issues,
1214 *Quaternary Science Reviews*, 24 (5-6), 595-629, 2005.

1215 WAIS Divide Project Members: Onset of deglacial warming in West Antarctica driven
1216 by local orbital forcing. *Nature*, 500, 440-444. doi:10.1038/nature12376, 2013.

1217 Xu, J., Kuhnt, W., Holbourn, A., Regenberg, M., and Andersen, N.: Indo-Pacific
1218 Warm Pool variability during the Holocene and Last Glacial Maximum, *Paleoceanogr.*,
1219 25, 16, 2010.

1220 Yamamoto, A., Abe-Ouchi, A., Ohgaito, R., Ito, A., and Oka, A.: Glacial CO₂
1221 decrease and deep-water deoxygenation by iron fertilization from glaciogenic dust,
1222 *Climate of the Past*, 15, 981-996.

1223 Yashayaev, I., Seidov, D., and Demirov, E.: A new collective view of oceanography
1224 of the Arctic and North Atlantic basins, *Progress in Oceanography*, 132, 21 pp.,
1225 DOI:<http://dx.doi.org/10.1016/j.pocean.2014.12.012>, 2015.

1226 Zhao, N. and Keigwin, L.D.: An atmospheric chronology for the glacial-deglacial
1227 Eastern Equatorial Pacific, *Nature communications*, 9:3077, DOI:10.1038/s41467-018-
1228 05574-x, 2018.

1229 Zhao, N., Marchal, O., Keigwin, L., Amrhein, D., and Gebbie, G.: A synthesis of
1230 deep-sea radiocarbon records and their (in) consistency with modern ocean ventilation,
1231 *Paleoceanography and Paleoclimatology*, 33, 128-151, 2018.

1232 TABLE CAPTIONS

1233

1234 **Table 1 a and b.** Summary of varve- and U/Th model-based age estimates (Schlolut
 1235 et al., 2018; Bronk Ramsey et al., 2012) for ~30 plateau (pl.) boundaries in the
 1236 atmospheric ¹⁴C record identified in Lake Suigetsu Core SG06₂₀₁₂ by means of visual
 1237 inspection over the interval 10.5–27 cal. ka (Sarnthein et al., 2015, suppl. and modified).
 1238 At the right hand side, three columns give the average (Ø) and uncertainty range of ¹⁴C
 1239 ages for each ¹⁴C plateau.

SUIGETSU Plateau Top	Depth	Plateau Base	Depth	Ø 14C Age	±Uncertainty	14C age BP			
SG06_2012	(cm c.d.)	(cm c.d.)	(cm c.d.)	of 14C Plateau	(14C yr)	min/max.			
Plateau no.	Varve-based age (yr BP)	U/Th-based age (yr BP)	Varve-based age (yr BP)	(14C yr)		(1.6 σ range)			
'Preboreal'	10525	10560	1325	11100	11108	1383	9525	-170/+110	9356/ 9635
'Top YD'	11290	11281	1402	11760	11755	1453	10060	-100/+35	9963/ 10095
'YD'	11950	11895	1467	12490	12475	1525	10380	-170/ 124	10211/ 10504
'no name'	12885	12780	1555	13160	13080	1582	11000	-85/ 114	10915/ 11114
1a	13580	13656	1626	13980	14042	1657	12006	100	11857/ 12050
1	14095	14160	1666	15095	15100	1740	12471	185	12315/ 12683
2a	15310	15420	1754	16140	16520	1802	13406	245	13174/ 13665
2b	16075	16520	1802	16400	16930	1820	13850	40	13808/ 13885
3	16835	17500	1847	17500	18220	1888	14671	105	14582/ 14792
4	17880	18650	1913	18830	19590	1971	15851	190	15661/ 16044

1240

5a	18960	19720	1978	19305	20240	2003	16670	90	16570/ 16750
5b	19305	20240	2003	20000	20900	2032	17007	190	16830/ 17247
6a	20190	21000	2050	20920	21890	2105	17667	262	17435/ 17960
6b	20920	21890	2105	21275	22300	2132	18075	140	17960/ 18240
7	21375	22400	2140	21790	22870	2171	18843	117	18741/ 18975
8	21835	22940	2175	22730	24250	2257	19715	-290 325	19425/ 20041
9	22730	24250	2257	23395	25150	2312	20465	-227 263	20238/ 20728
10a	23935	25880	2358	25080	27000	2400	22328	-380 270	21946/ 22600
10b	25080	27000	2400	25800	27600	2426	22708	-475 440	22233/ 23147
11	26110	27770	2443	27265	28730	2525	24088	-360 505	23727/ 24595

1241

1242

1243 **Table 2.** Temporal match of various ¹⁴C plateaus with deglacial periods of major
 1244 atmospheric CO₂ rise and ocean warmings (AA = Antarctic; GIS = Greenland
 1245 Interstadial).

pCO ₂ RISE (~12 ppm)	Plateau no.	Plateau boundaries
AGE based on annual layers AA ice core (Marcott et al. 2014)		AGE range (cal. ka) based on U/Th model ages (Bronk Ramsey et al., 2012)
11.7 – 11.5	# 'Top YD'	11.83 – 11.3
14.8 – 14.53	# 1	15.1 – 14.2
16.4 – 16.15	# 2a	16.52 – 15.5
17.4 – ~17.1	(data gap)	17.3 – 17.1

FURTHER POTENTIAL CORRELATIVES:

Progressive N. Atlantic warming during the YD at 12.39 – 12.03 ka *	# 'YD'	12.46 – 11.98
Onset of Antarctic ** warming at 18.3–17.6 ka (ice-based time scale)	#3	18.22 – 17.5
Onset of North Atlantic *** warming at 19.3–18.6 ka (U/Th-based time scale)	# 4	19.6 – 18.65
Top H2: GIS 2 N. Atlantic warming at 23.4 – 23.3 ka ****	#8	24.25 – 22.95

AGE CONTROL based on

* Naughton et al. (2019), ** Kawamura et al. (2007),

*** Balmer and Sarnthein (2018), **** Grootes and Stuiver (1997)

1246

1247 **Table 3** a-c. ¹⁴C reservoir / ventilation ages of surface (top 50-100 m) and bottom
 1248 waters vs. U/Th-based model age at 19/22 core sites in the ocean. (a) Spatial and
 1249 temporal changes over early and late LGM (24–21 and 21–18.7 cal. ka), (b) HS-1, and
 1250 the B/A. Late LGM estimates (average res. age of Plateau 4-5) are compared to model-
 1251 based estimates of Muglia et al. (2018). (c) Data sources. For core locations see Fig. 7.
 1252 (a)

Sediment Core U/Th-based model age Plateau (Pl.) no.	Latitude	Longitude	Water depth (m)	LGM pla. res. age		LGM model		res. age	
				24–21 ka (early LGM) Pl. 8 - 7 - 6 Error (yr)	21–18.7 ka (late LGM) Pl. 5 - 4 Error (yr)	strong AMOC (yr)	weak (yr)		
ATLANTIC O.									
PS2644	67°52.02'N	21°45.92'W	777	2100	±390	1920–2200	±325 –±12!	1136	1100
GIK 23074	66°66.67'N	4°90'E	1157	620–790	±145–±270	550–1175	±100–±200	1054	1059
MD08-3180	38°N	31°13.45'W	3064	–	–	320–605	±125–±405	827	887
SHAK06-5K (= MD99-2334)	37°34'N (37°48'N)	10°09'W 10°10'W	2646 3146	675–800	–	500–660	–	872	855
ODP 1002	10°42.37'N	65°10.18'W	893	700–210	±230–±310	25 – -205	±205–±215	751	738
GeoB 3910-1	4°15'S	36°21'W	2361	–	–	–	–	779	796
GeoB 1711-4	23°17'S	12°23'W	1976	1080	±290	730–840	±240–±190	711	721
KNR 159-5-36GGC	27°31'S	46°48'W	1268	540	±140	870	±120	757	777
MD07-3076	44°4'S	4°12'W	3770	–	–	2300	±200	928	989
INDIAN O./TIMOR SEA									
MD01-2378	13°08.25'S	121°78.8'E	1783	–	–	2000–1700	±300–±320	885	890
PACIFIC O.									
MD02-2489	54°39.07'N	148°92.13'W	3640	–	–	1560–1110	±310–±335	972	965
MD01-2416	51°26.8'N	167°72.5'E	2317	–	–	1710	±440	1227	1202
ODP 893A	34°17.25'N	120°02.33'W	588	–	–	1065	±280	839	846
MD02-2503	34°16.6'N	120°01.6'W	580	–	–	–	–	839	846
GIK 17940	20°07.0'N	117°23.0'E	1727	1820–1260	±320–±230	hiatus	–	836	838
(= SO50-37)	18°55'N	115°55'E	2655	1820–1260	–	–	–	836	840
PS75/104-1	44°46'S	174°31'E	835	1650–1280	±210–±320	1500	±340	881	895
(= SO213-84)	45°7.5'S	174°34,9'E	972	1650–1280	±210–±320	1500	±340	881	895
MD07-3088	46°S	75°W	1536	385	±315	380-450	±140–±230	917	–
SO213-76-2	46°13'S	178°1.7'W	4339	–	–	1460–990	±340–±550	915	842
PS97/137-1	52°39.5'S	75°33.9'E	1027	600–1180	±465	1180–800	±90–±225	1505	1419

1253

1254 (b)

Sediment Core U/Th-based model age Plateau (Pl.) no.	HS-1 pla. res. age		16.5–15.5 ka		B/A pla. res. age		LGM be. vent age		LGM b.w. model age	
	Pl. 3 - 2b (yr)	Error (yr)	Pl. 2a (yr)	Error (yr)	Pl. 1 - 1a	Error (yr)	early	late	strong AMOC (yr)	weak (yr)
ATLANTIC O.										
PS2644	1775–1660	±105–±160	1900	±355	–	–	345	2400	948	918
GIK 23074	1730–2000	±125–±160	670	±310	140–310	±250–±100	375	375	960	931
MD08-3180	1420–1610	±310–±160	1460	±390	630–360	±310	600	600	1031	1004
SHAK06-5K (= MD99-2334)	330–410	–	535	–	780–925	–	–	–	–	–
ODP 1002	–100 – 20	±140	90	±345	355	±200	–	–	1247	1175
GeoB 3910-1	630–560	±160–±180	175	±475	210–230	±220–±110	2150	2150	–	–
GeoB 1711-4	660–690	±195–±45	420	±320	880	±255	1500	1500	1387	1714
KNR 159-5-36GGC	460–340	±380–±300	170	±700	180–230	±370–±310	1470	1470	1354	1563
MD07-3076	1650	±180	–	–	920	±230	3640	3640	1653	2060
INDIAN O./TIMOR SEA										
MD01-2378	740	±125	–	–	200–185	±345–±130	2720	–	1679	1881
PACIFIC O.										
MD02-2489	800–550	±155–±120	550	±305	440	±285	–	2625	2332	2595
MD01-2416	1480–1140	±135–±190	–	–	720–570	±285–±140	–	3700/5100	2400	2683
ODP 893A	1065–1490	±280–±120	1400	±370	520	±185	–	1430	1677	1705
MD02-2503	965–1365	±160–±160	1215	±325	395–535	±240–±130	–	–	–	–
GIK 17940 (= SO50-37)	1210–1370	±200–±470	1045	±320	870–970	±325–±100	3300–1800	–	1807	1897
PS75/104-1 (= SO213-84)	1050	±265	1180	±350	800	±280	–	–	–	–
MD07-3088	800–1090	±85–±125	1060	±275	1310–730	±125–±190	1360 ?	1600	1101	1146
SO213-76-2	840	±310	–	–	–	–	–	3460	1808	1701
PS97/137-1	1500–670	±90–±180	455	±270	–	–	1400–2400	2400/2900	1712	2001
									1631	1871

1255

1256 (c)

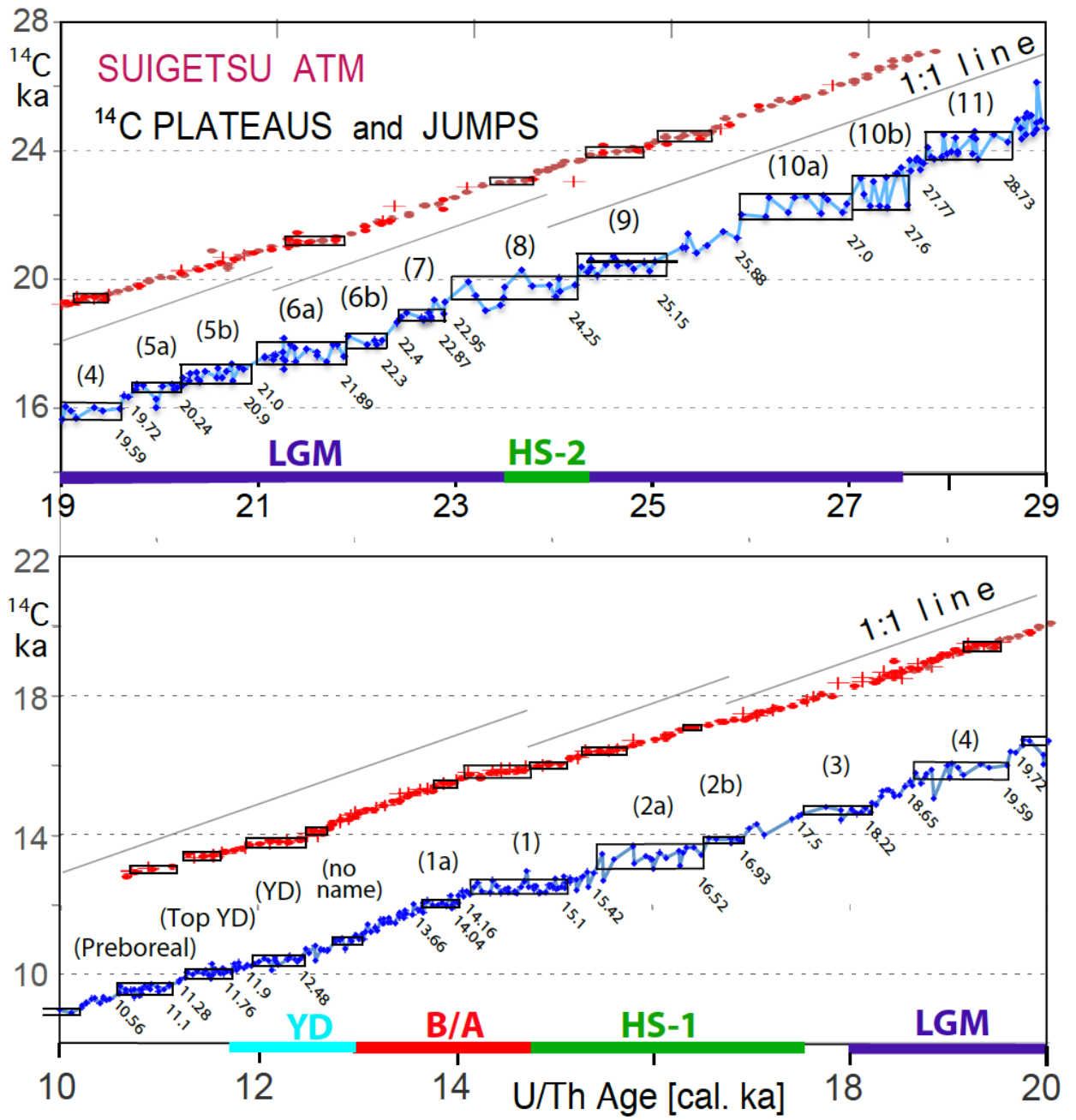
Sediment Core	DATA Source
ATLANTIC O.	
PS2644	Sarnthein et al. 2015 Be.data suppl.
GIK 23074	Sarnthein et al. 2015 Be.data suppl.
MD08-3180	Balmer et al. 2018
SHAK06-5K (= MD99-2334)	Ausin et al., 2020 subm. Skinner et al. 2014
ODP 1002	Sarnthein et al. 2015
GeoB 3910-1	Balmer et al. 2016
GeoB 1711-4	Balmer et al. 2016
KNR 159-5-36GGC	Balmer et al. 2016 data suppl.
MD07-3076	Balmer et al. 2016
INDIAN O./TIMOR SEA	
MD01-2378	Sarnthein et al. 2015
PACIFIC O.	
MD02-2489	Sarnthein et al. 2015
MD01-2416	Sarnthein et al. 2015 modified
ODP 893A	Sarnthein et al. 2015 data suppl.
MD02-2503	Sarnthein et al. 2015
GIK 17940 (= SO50-37)	Sarnthein et al. 2015
PS75/104-1 (= SO213-84)	Küssner et al., 2018+2020 Ronge et al., 2016
MD07-3088	Küssner et al., 2020 subm Siani et al. 2013
SO213-76-2	Küssner et al., 2020 subm Ronge et al. 2016
PS97/137-1	Küssner et al., 2020 subm data suppl.

1257 (c)

1258 FIGURE CAPTIONS

1259

1260 – Fig. 1. Atmospheric ^{14}C ages of Lake Suigetsu plant macrofossils 10–20 cal. ka
1261 (bottom panel) and 19–29 cal. ka (top panel) vs. U/Th-based model age (blue dots;
1262 Bronk Ramsey et al., 2012). The 1:1 line reflects gradient of one ^{14}C yr / cal. yr. Double
1263 and triple ^{14}C measurements are averaged. (In part large) error bars of single ^{14}C ages
1264 are given in Suppl. Fig. S1. Suite of labeled horizontal boxes that envelop scatter bands
1265 of largely constant ^{14}C ages shows ^{14}C plateaus longer than 250 yr (plateau boundary
1266 ages listed in Table 1). Red and brown dots (powder samples from trench and wall) and
1267 + signs (off-axis samples) depict raw ^{14}C ages of Hulu stalagmites H82 and MSD
1268 (Cheng et al., 2018; Southon et al., 2012; plot offset by +3000 ^{14}C yr). Suite of short ^{14}C
1269 plateaus (black boxes) tentatively assigned to Hulu-based record occupies age ranges
1270 slightly different from those deduced for Suigetsu-based plateaus. The difference
1271 possibly results from short-term changes in the Old / Dead Carbon Fraction (ocf / dcf)
1272 that in turn may reflect major short-term changes in LGM and deglacial monsoon
1273 climate (Wang et al., 2001; Kong et al., 2005).

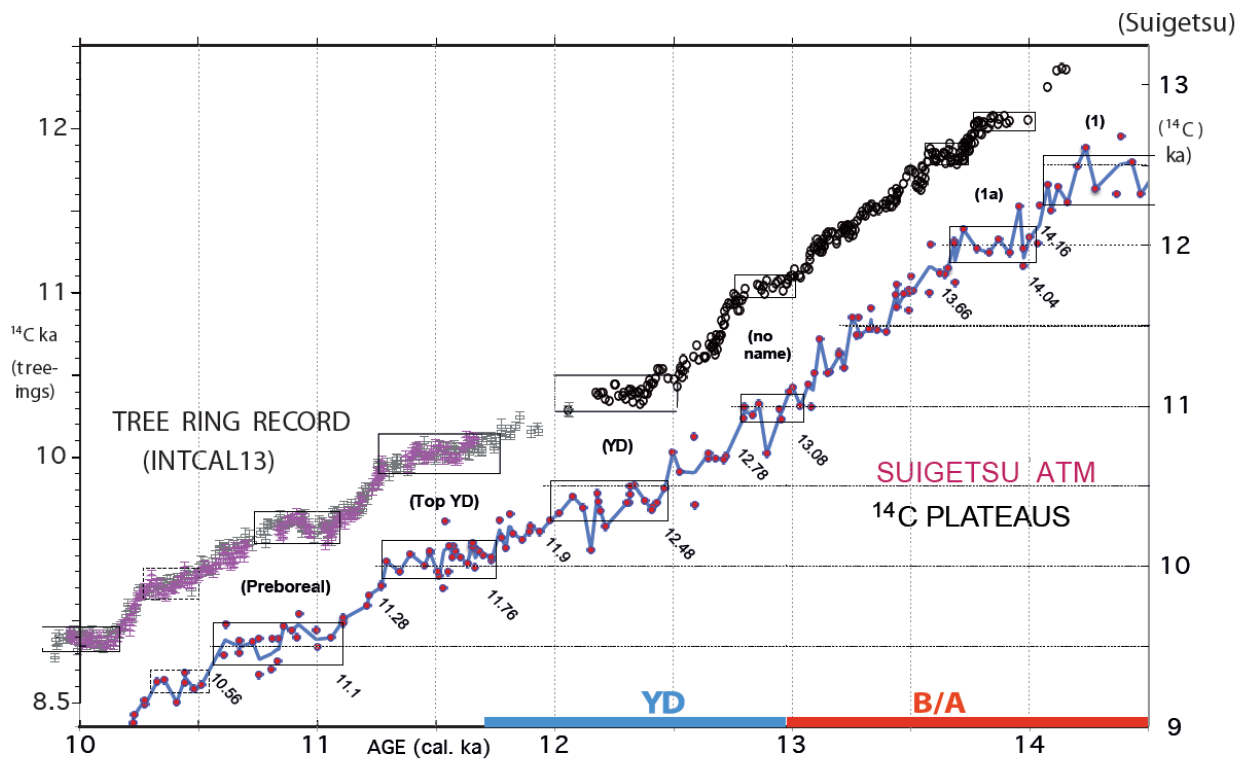


1274

1275

1276

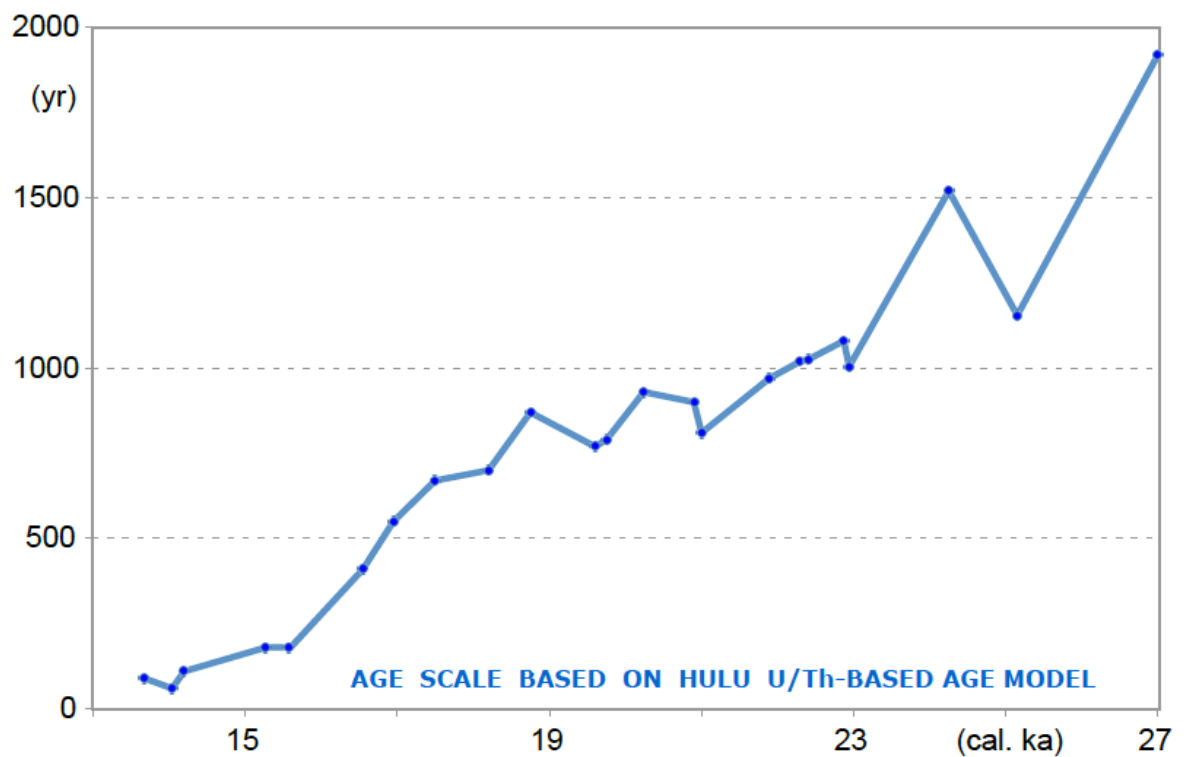
1277 ✕ Fig. 2. High-resolution record of atmospheric ^{14}C jumps and plateaus (= suite of
 1278 labeled horizontal boxes that envelop scatter bands of largely constant ^{14}C ages
 1279 extending over >300 cal. yr) in a sediment section of Lake Suigetsu vs. tree ring-based
 1280 ^{14}C jumps and plateaus 10–14.5 cal. ka (Reimer et al., 2013). Blue line averages paired
 1281 double and triple ^{14}C ages of Suigetsu plant macrofossils. Age control points (cal. ka)
 1282 follow varve counts (Scholout et al., 2018) and U/Th model-based ages of Bronk
 1283 Ramsey et al. (2012). YD = Younger Dryas, B/A = Bølling-Allerød.
 1284



1285
 1286
 1287
 1288
 1289
 1290
 1291
 1292
 1293
 1294
 1295

1296 ✖ Fig. 3. Difference between Hulu Cave U/Th-based model ages (Southon et al., 2012;
1297 Bronk Ramsey et al., 2012; Cheng et al., 2018) and varve count-based cal. ages for
1298 atmospheric ^{14}C plateau boundaries in Lake Suigetsu sediment record (Schlolut et al.,
1299 2018) (Sarnthein et al., 2015, suppl. and revised), displayed on the U/Th-based time
1300 scale 13–27 cal. ka.

1301



1302

1303

1304

1305

1306

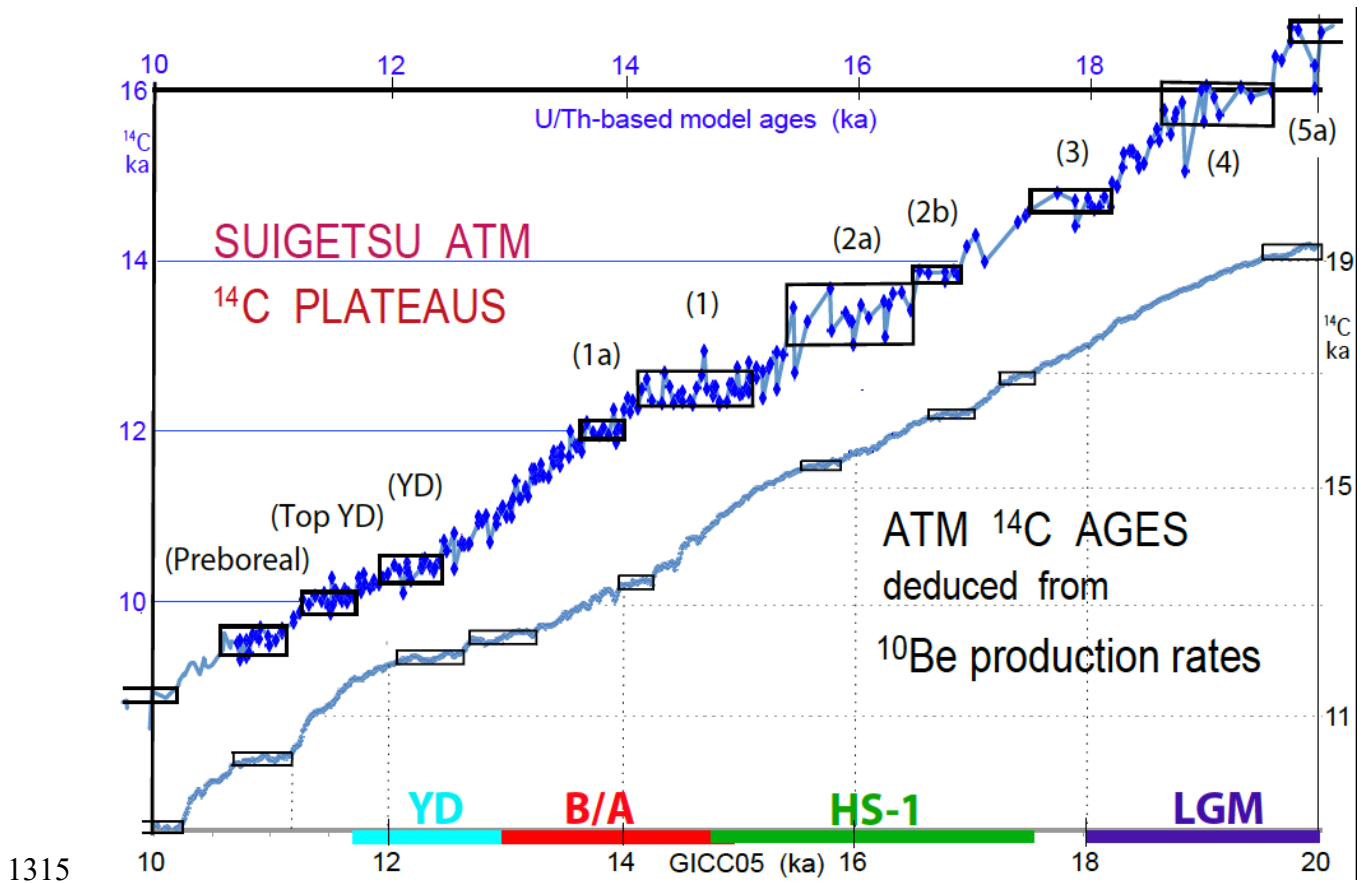
1307

1308

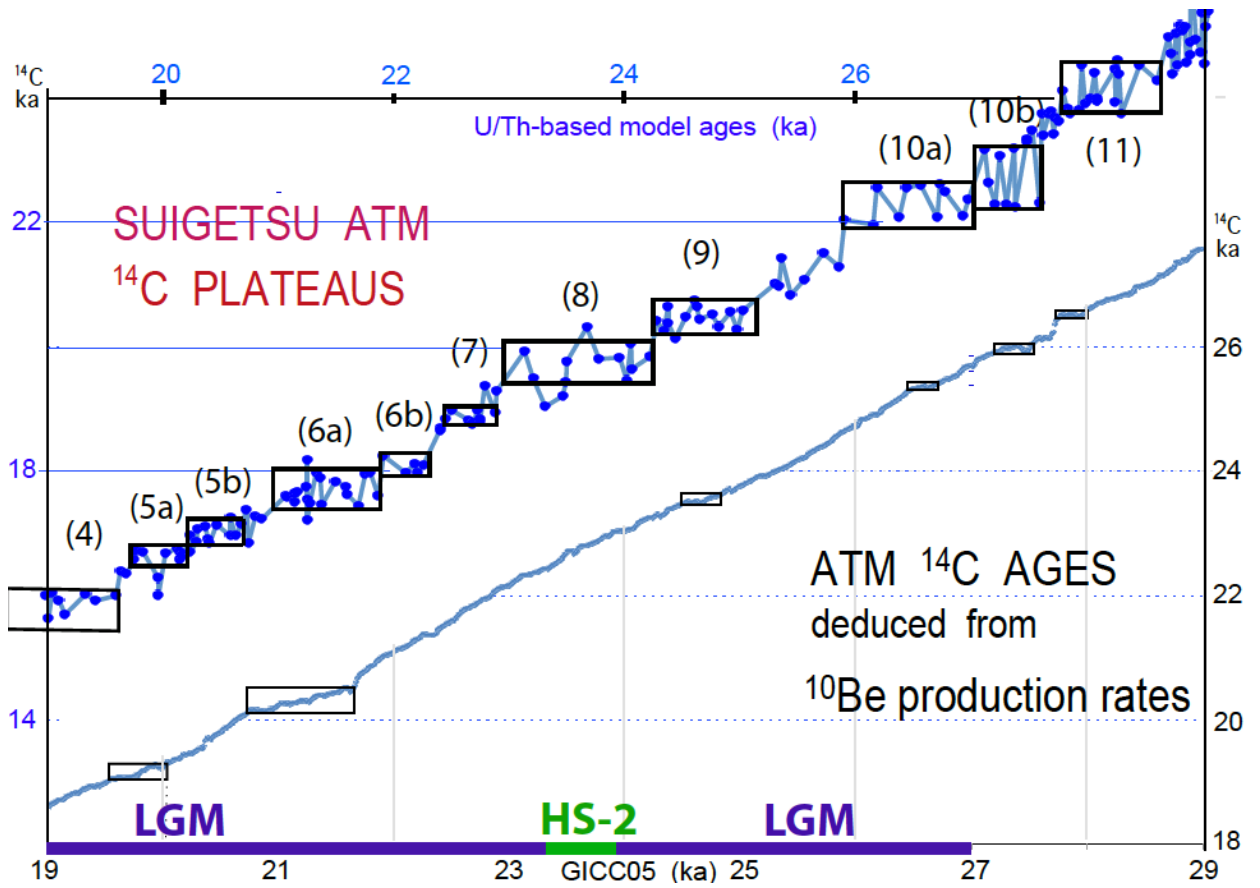
1309

1310

1311 √ Fig. 4 a and b. Atmospheric ^{14}C ages and plateaus (horizontal boxes) deduced from
 1312 ^{10}Be production rates vs. GICC05 age scale (Adolphi et al., 2018) compared to the
 1313 Suigetsu record of atmospheric ^{14}C plateaus vs. Hulu U/Th-based model ages (Southon
 1314 et al., 2012; Cheng et al., 2018) for the intervals a) 10-20 and b) 19-29 cal ka BP.



1315



1316

1317

1318

1319

1320

1321

1322

1323

1324

1325

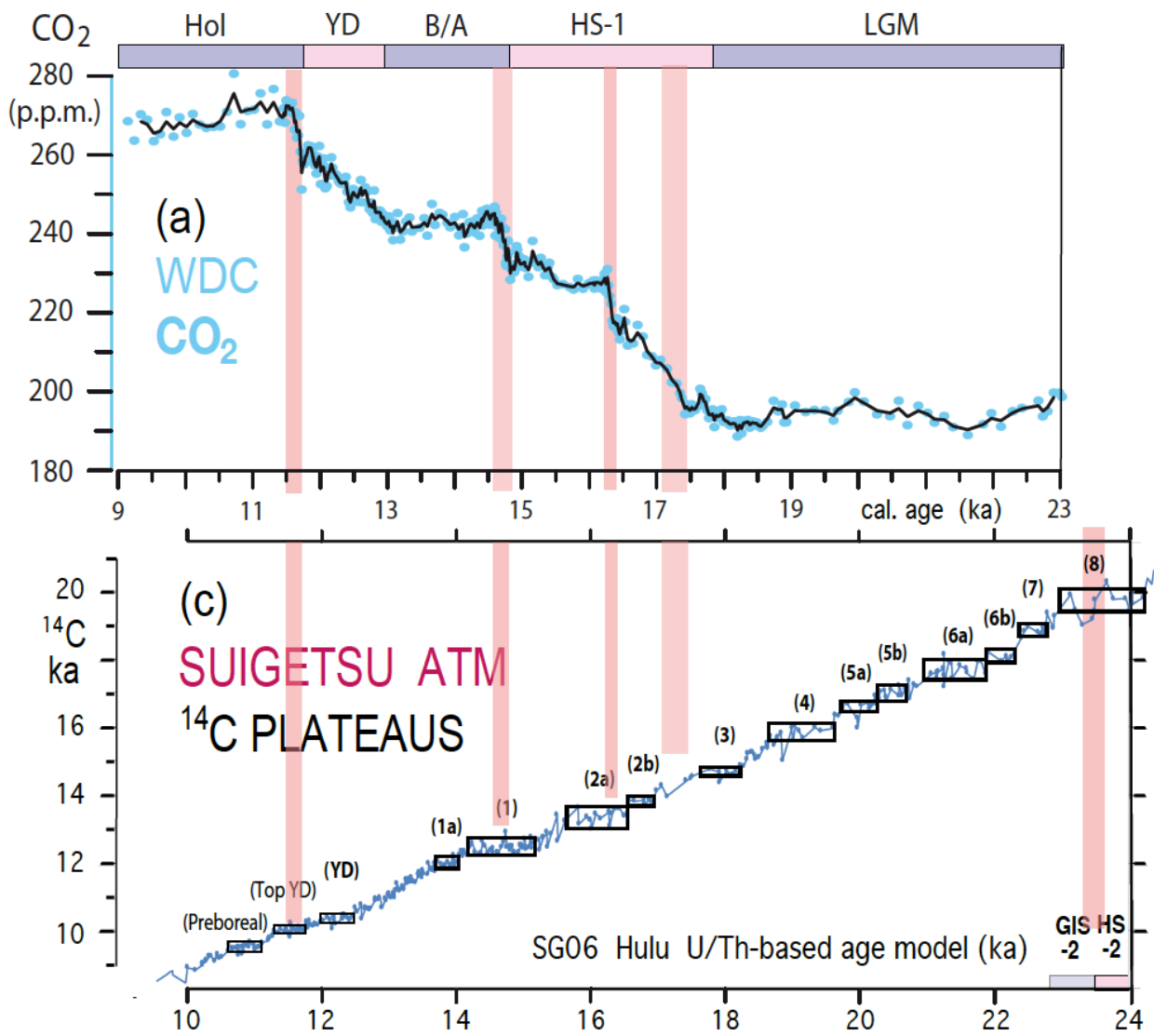
1326

1327

1328

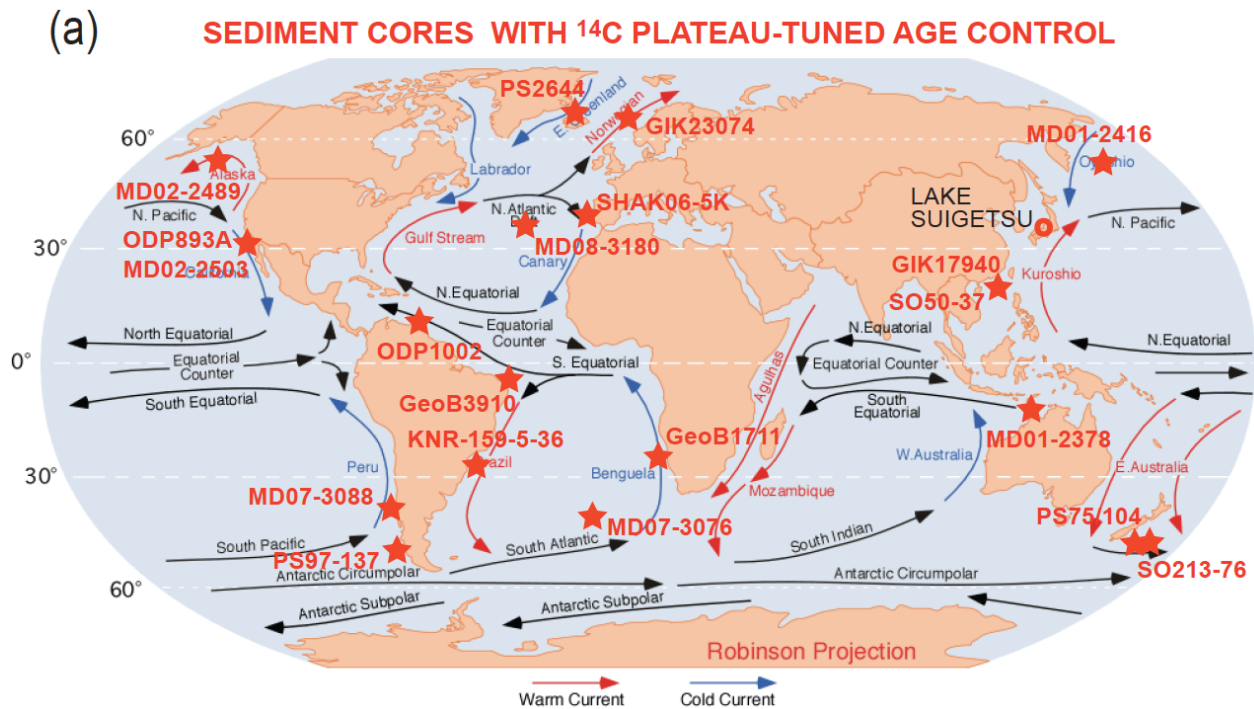
1329

1340 ✗ Fig. 6 (a). Four sudden steps (pink bars) in the deglacial atmospheric CO₂ rise at
 1341 West Antarctic Ice Sheet Divide ice core (WDC) reflect events of fast ocean degassing,
 1342 that may have contributed to the origin of deglacial ¹⁴C plateaus. Age control based on
 1343 ice cores (Marcott et al., 2014). (b) The steps are compared to suite of atmospheric ¹⁴C
 1344 plateaus dated by Hulu U/Th-based model ages (Bronk Ramsey et al., 2012). Hol =
 1345 Holocene; YD = Younger Dryas; B/A = Bølling-Allerød; HS = Heinrich stadials 1 and 2;
 1346 LGM = Last Glacial Maximum, GIS-2 = Greenland interstadial 2.
 1347

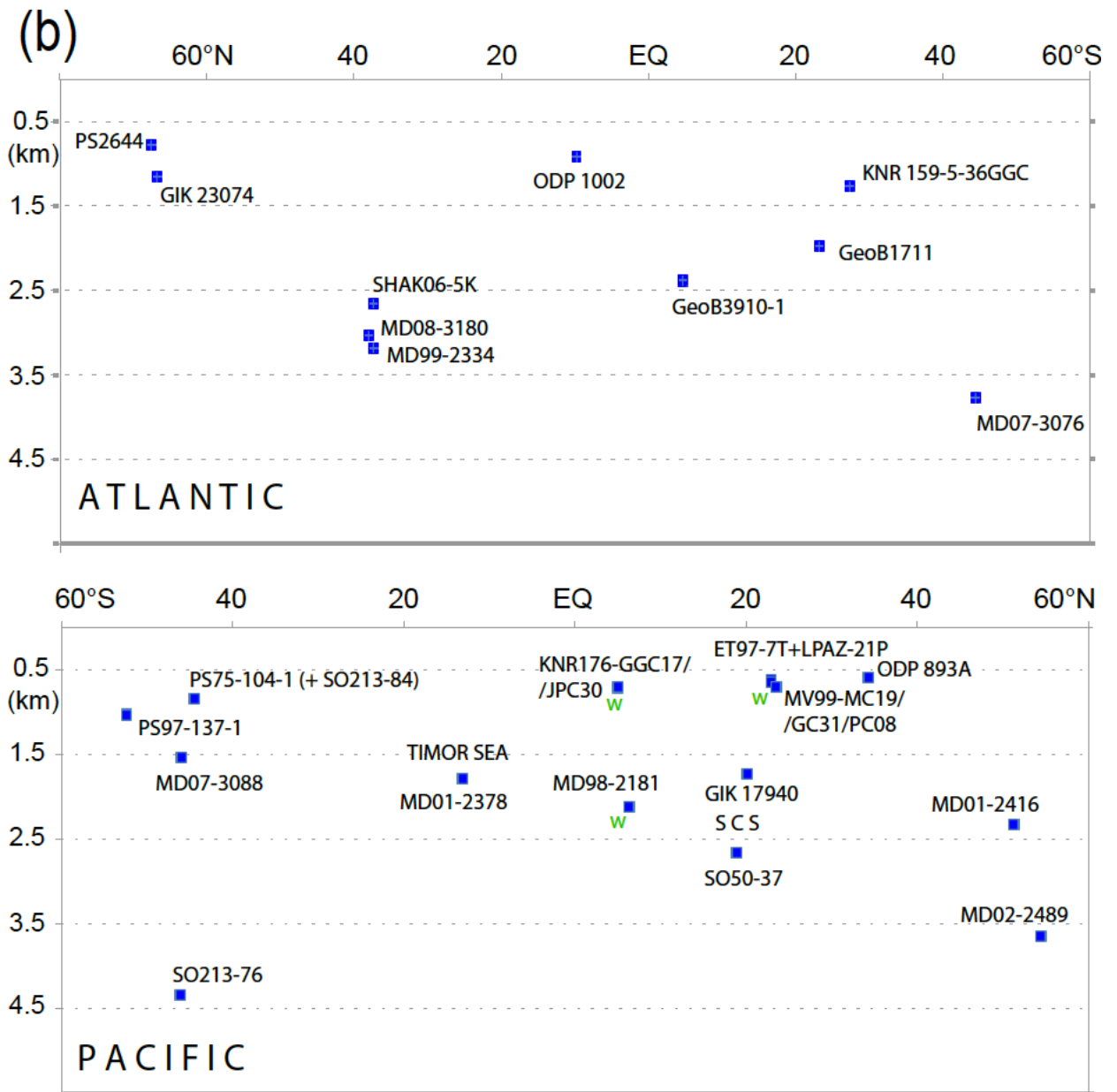


1348
 1349

1350 ✕ Fig. 7. Location (a) and water depth (km) (b) of sediment cores with age control based
 1351 on ¹⁴C plateau tuning. ¹⁴C reservoir ages of cores labeled with 'w' are derived from
 1352 samples with paired wood chunks and planktic foraminifers.



1353



1354

1355

1356 √ Fig. 8. Global distribution of ^{14}C reservoir ages of Late LGM surface waters estimated

1357 (a) by means of ^{14}C plateau tuning of planktic ^{14}C records. (b) Model-based estimates

1358 (GCM of Muglia et al., 2018, assuming an AMOC strength of 13 Sv) for sites with

1359 planktic foraminifera-based age values. X-Y graph (c) and map (d) show (rounded)

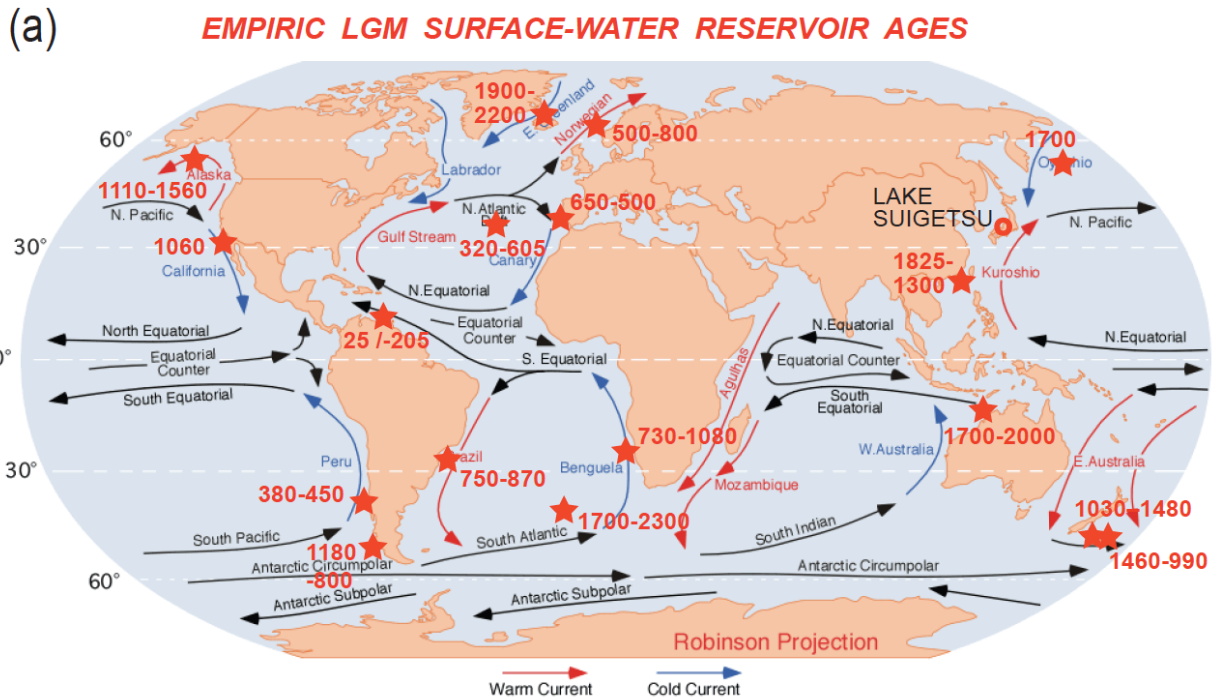
1360 differences between observed and modeled values and their intra-LGM trends. Minor

1361 differences are displayed in magenta, larger differences of >400 yr in red. Planktic

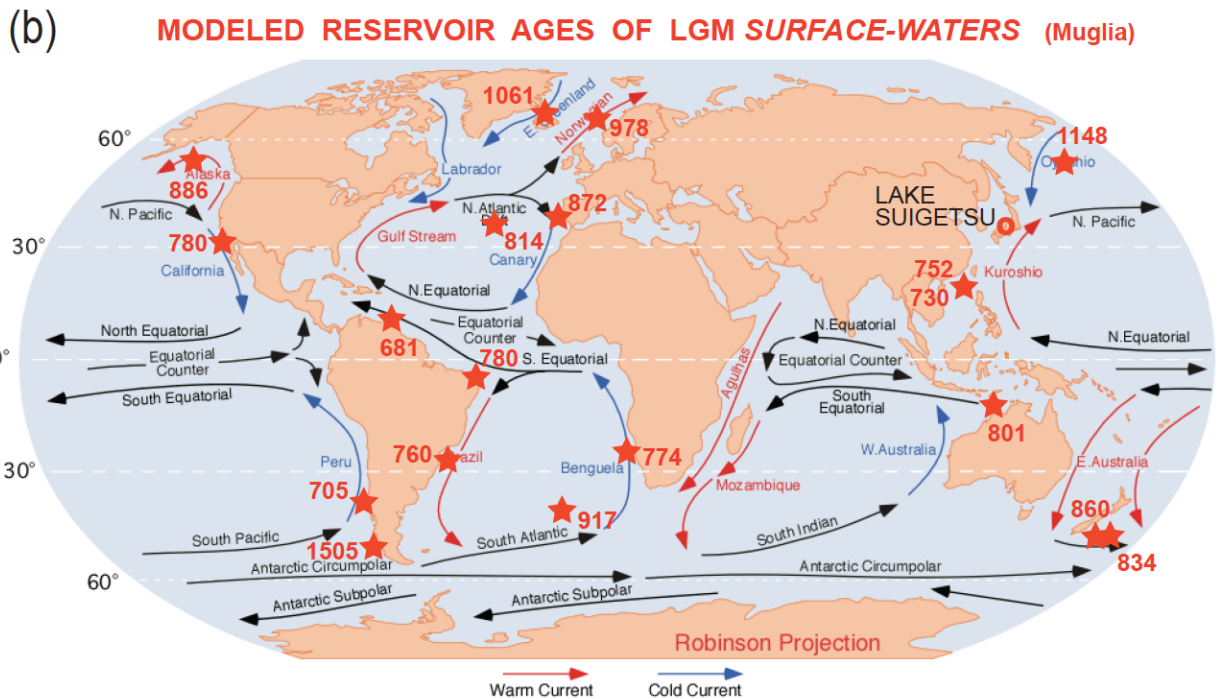
1362 habitat depths and model estimates are largely confined to 0–100 m water depth.

1363 Arrows of surface currents delineate different sea regions important to assess potential
 1364 limits of spatial extrapolation of reservoir ages. Distribution of core numbers and
 1365 references for ¹⁴C records are given in Table 3a-c and Fig. 7a.

Fig. 8a

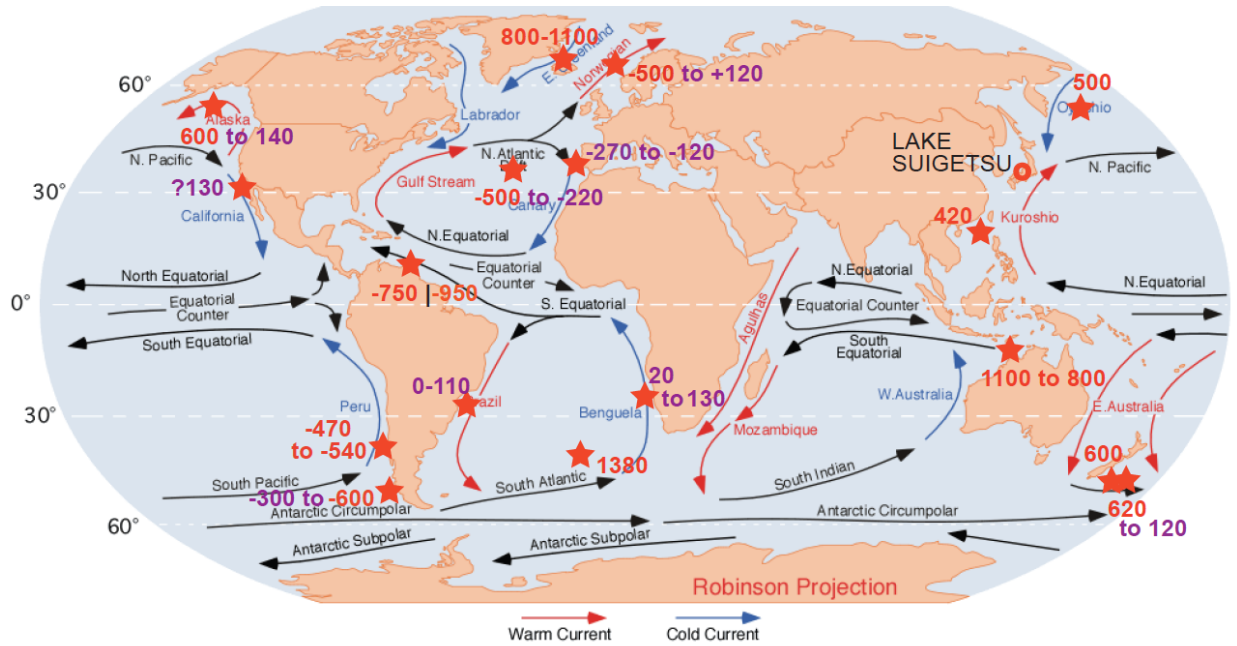


1366



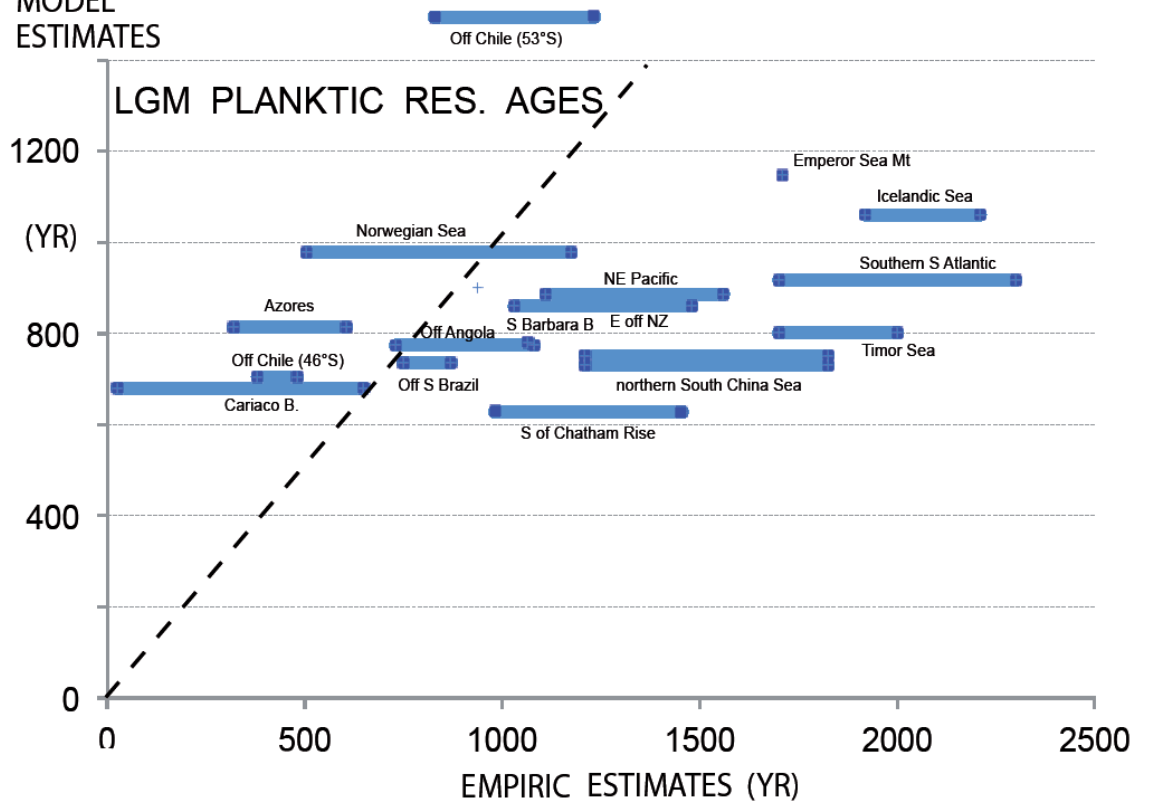
1367

(c) **EMPIRIC minus Muglia MODEL RESERVOIR AGES (yr) of LGM S.W.**



1368

(d) **MODEL ESTIMATES**

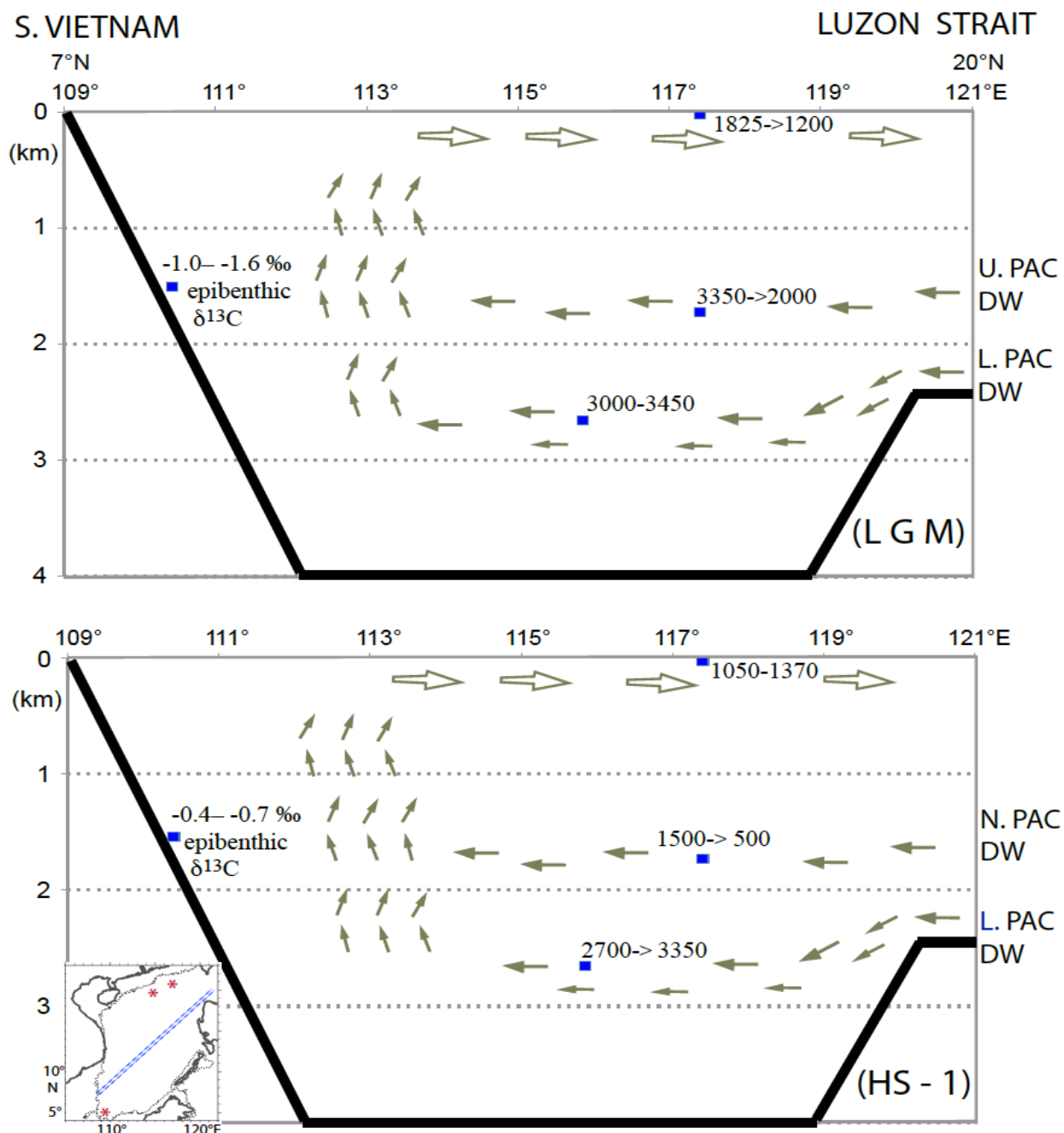


1369

1370

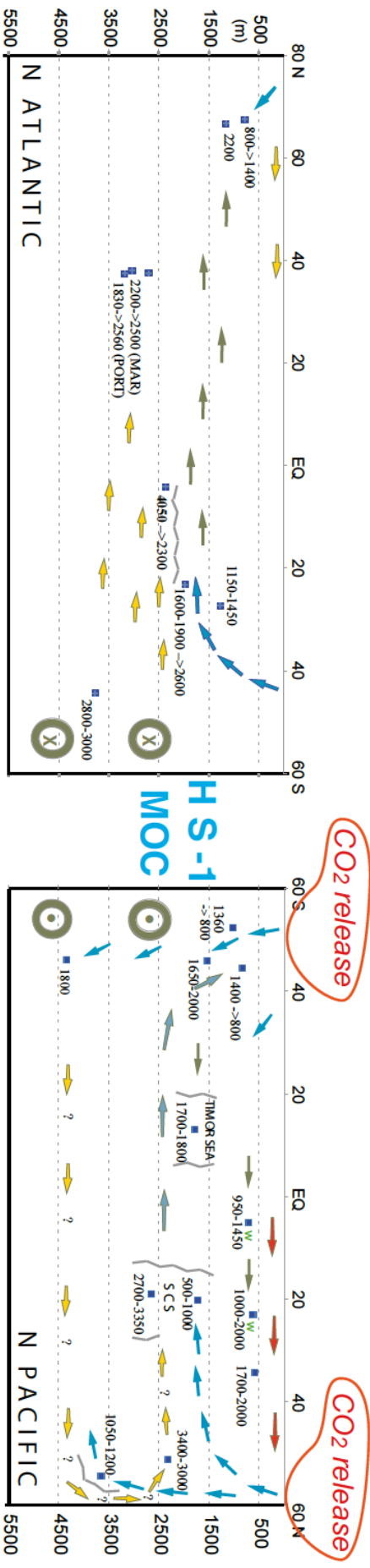
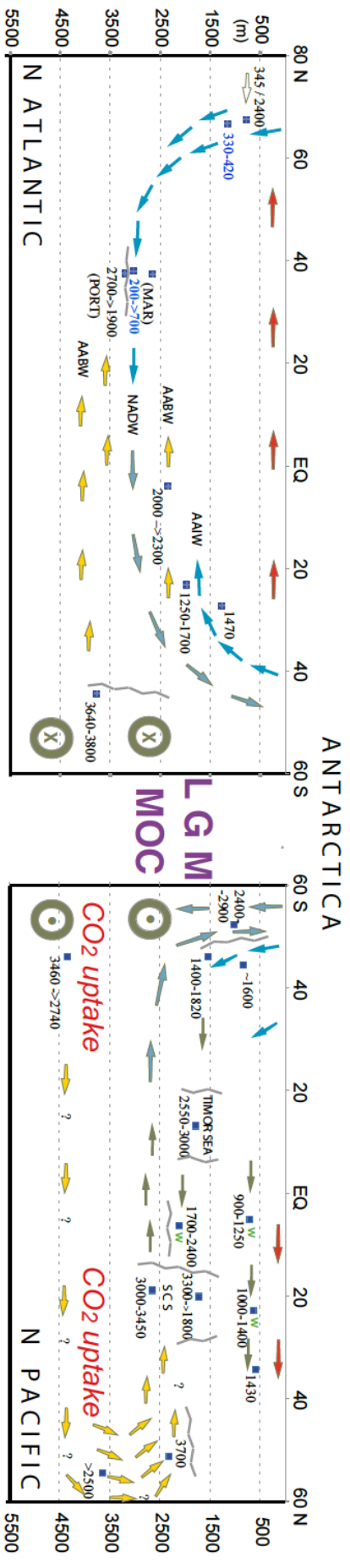
1371 √ Fig. 9. SW–NE transect of ^{14}C reservoir age and changes in ventilation age across
 1372 sites GIK17940 and SO50-37 in the South China Sea during late LGM (^{14}C Plateaus 5

1373 and 4; upper panel) and HS-1 (lower panel). Insert map shows location of transect and
 1374 core locations. Core locations are given in Fig. 7. An extreme epibenthic $\delta^{13}\text{C}$ minimum
 1375 in far southwest (Core GIK17964; Sarnthein et al., 1999) reflects an LGM incursion of
 1376 Lower/Upper Pacific Deep Waters (L./ U. PAC DW) with extremely high ^{14}C ventilation
 1377 age and DIC enrichment in contrast to a low ventilation age of North Pacific Deep Water
 1378 (N. PAC DW). Arrows show direction of potential deep and intermediate-water currents.



1379

1380 ✗ Fig. 10. 2D transects of the geometries of global ocean MOC. Arrows (blue = high,
1381 yellow = poor ventilation) suggest average deep and intermediate-water currents that
1382 follow the gradient from low to high benthic ventilation ages based on paired planktic
1383 ¹⁴C reservoir ages derived by means of ¹⁴C plateau tuning technique (Sarnthein et al.,
1384 2013, Balmer et al., 2018, Küssner et al., 2020 subm.). At some Pacific sites reservoir
1385 ages are based on paired ¹⁴C ages of planktic foraminifera and wood chunks (marked
1386 by green 'w'; Sarnthein et al., 2015; Zhao and Keigwin, 2018, Rafter et al., 2018). Red
1387 arrows suggest poleward warm surface water currents. Zigzag lines indicate major
1388 frontal systems separating counter rotating ocean currents (e.g., W of Portugal and N of
1389 MD07-307; after Skinner et al., 2014). (a) Late LGM circulation geometry (21–18.7 cal.
1390 ka), largely similar to today. Note the major east-west gradient of ventilation ages in the
1391 central North Atlantic, between Portugal (PORT) and Mid-Atlantic Ridge W of Azores
1392 (MAR). (b) HS-1 benthic ventilation ages reveal a short-lasting MOC reversal leading to
1393 Atlantic-style overturning in the subpolar North Pacific and coeval Pacific-style stratific-
1394 ation in the northern North Atlantic, with seesaw-style reversals of global MOC at the
1395 onset and end of early HS-1 (first proposed by Broecker et al., 1985, however, for LGM
1396 times). Increased ventilation ages reflect enhanced uptake of dissolved carbon in the
1397 LGM deep ocean (Sarnthein et al., 2013), major drops suggest major degassing of CO₂
1398 from both the deep Southern Ocean and North Pacific during early HS-1. – SCS =
1399 South China Sea. AABW = Antarctic Bottom Water; AAIW = Antarctic Intermediate
1400 Water. NADW = North Atlantic Deep Water. Small arrows within age numbers reflect
1401 temporal trends. Many arrows are speculative using circumstantial evidence of benthic
1402 δ¹³C records and local Coriolis forcing at high-latitude sites per analogy to modern
1403 scenarios. Location of sediment cores are given in Fig. 7, short-term variations in
1404 planktic and benthic ¹⁴C reservoir/ventilation age in Suppl. Fig. S2 and Table 3.

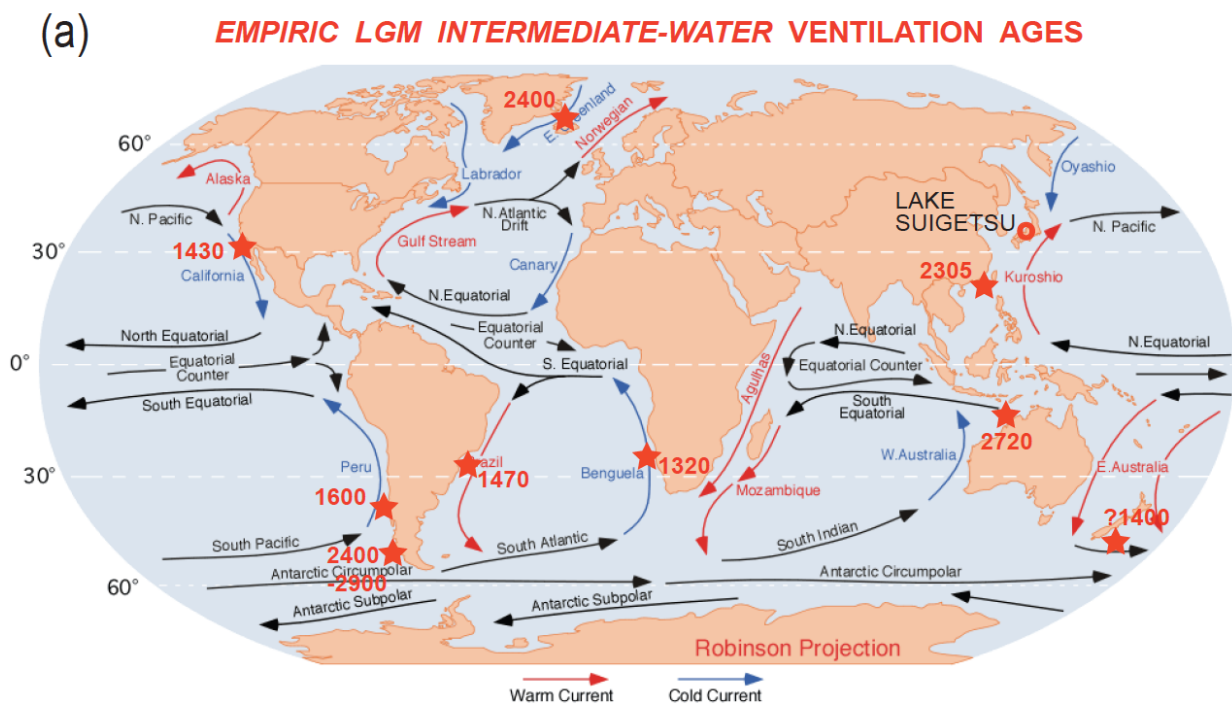


1406

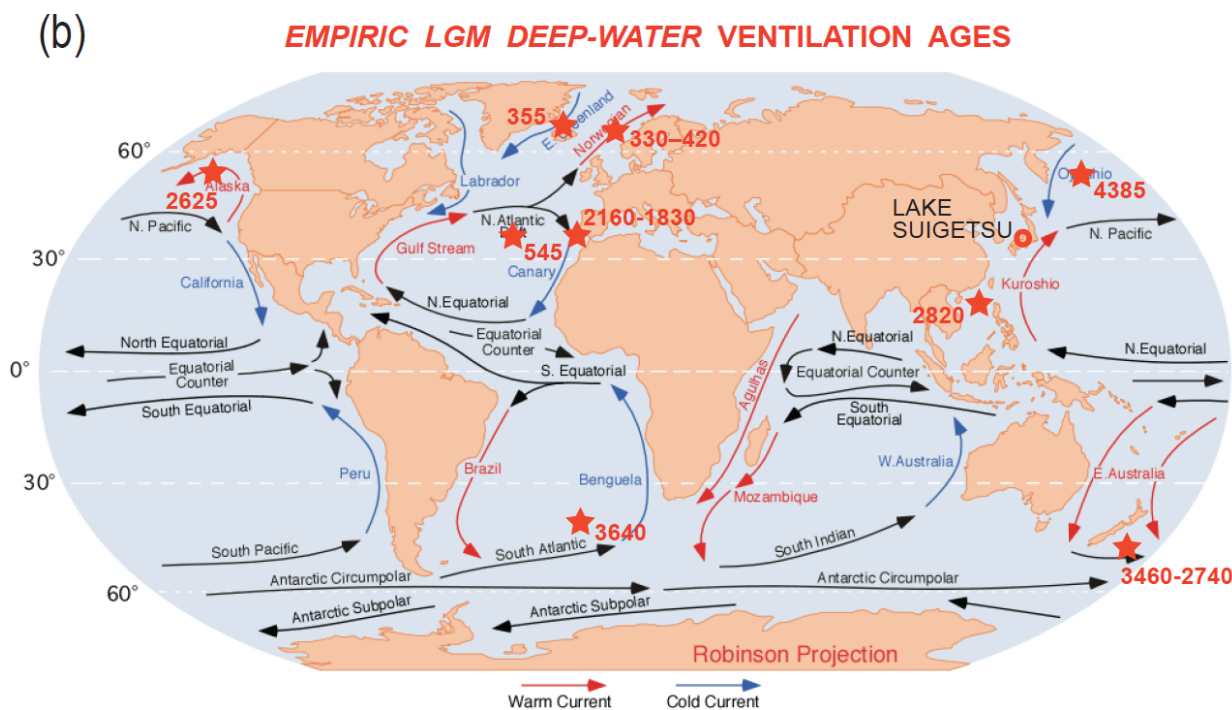
1407 √ Fig. 11. Global distribution of ¹⁴C reservoir ages obtained (a) for late LGM

1408 intermediate waters (100–1800 m w.d.) and (b) for LGM deep waters (>1800 m w.d.),

1409 including Site GIK 23074 at 1157 m in the Norwegian Sea).



1410



1411